

Parameter dependence of magnetized CMB observables

Massimo Giovannini ¹

Department of Physics, Theory Division, CERN, 1211 Geneva 23, Switzerland

INFN, Section of Milan-Bicocca, 20126 Milan, Italy

Abstract

Pre-decoupling magnetic fields affect the scalar modes of the geometry and produce observable effects which can be constrained also through the use of current (as opposed to forthcoming) data stemming from the Cosmic Microwave Background observations. The dependence of the temperature and polarization angular power spectra upon the parameters of an ambient magnetic field is encoded in the scaling properties of a set of basic integrals whose derivation is simplified in the limit of small angular scales. The magnetically-induced distortions patterns of the relevant observables can be computed analytically by employing scaling considerations which are corroborated by numerical results. The parameter space of the magnetized Cosmic Microwave background anisotropies is also discussed in the light of the obtained analytical results.

¹Electronic address: massimo.giovannini@cern.ch

1 Formulation of the problem

There are two complementary approaches to the analysis of the Cosmic Microwave Background (CMB in what follows) observables. The first one is direct and it consists in computing the angular power spectra by faithfully including all the relevant physical effects. The second approach is indirect, i.e. it amounts to deriving the dependence of the (measured) temperature and polarization anisotropies upon the parameters of the underlying model which needs to be falsified. The recent WMAP 5yr data [1, 2, 3] (see also [4, 5]) have been confronted with a number of theoretical scenarios that are logically organized around the Λ CDM paradigm where Λ stands for the dark-energy component and CDM stands for Cold Dark Matter. Similar statements can be made for other recent CMB data such as the ACBAR observations [6, 7] and the QUAD measurements [8, 9, 10, 11].

A useful bridge between the direct and the indirect approach is represented by a number of scaling relations which serve as a diagnostic for the dependence of the (observed) angular power spectra upon the parameters of a pivotal model. The temperature and polarization autocorrelations (i.e., respectively, TT and EE angular power spectra) and their mutual cross-correlations (i.e. the TE angular power spectra) can be written, with shorthand notation, as

$$G_\ell^{(\text{TT})} = \frac{\ell(\ell+1)}{2\pi} C_\ell^{(\text{TT})}, \quad G_\ell^{(\text{EE})} = \frac{\ell(\ell+1)}{2\pi} C_\ell^{(\text{EE})}, \quad G_\ell^{(\text{TE})} = \frac{\ell(\ell+1)}{2\pi} C_\ell^{(\text{TE})}. \quad (1.1)$$

In the Λ CDM scenario the angular power spectra of Eq. (1.1) are functions of, at least, six physical quantities

$$G_\ell^{(\text{XY})} = G_\ell^{(\text{XY})}(n_s, \Omega_{\text{b}0}, \Omega_{\text{c}0}, \Omega_\Lambda, H_0, \epsilon_{\text{re}}), \quad (1.2)$$

where X and Y stand, respectively, for T and E and where the parameters denote, with standard notations, the spectral index of (adiabatic) curvature perturbations (i.e. n_s), the critical fractions of baryons, CDM and dark energy (i.e., respectively, $\Omega_{\text{b}0}$, $\Omega_{\text{c}0}$ and Ω_Λ), the Hubble constant H_0 and the optical depth at reionization (i.e. ϵ_{re}).

In the Λ CDM paradigm as well as in its extensions, the known scaling relations are often not the result of a numerical inference but are derived by means of analytical methods. Suppose, for sake of concreteness, that all the parameters of Eq. (1.2) are fixed to the best fit of the WMAP 5yr data alone and just one (e.g. the spectral index) is allowed to scale. From semi-analytic considerations it follows that

$$G_\ell^{(\text{TT})} \propto \left(\frac{\ell}{\ell_{\text{p}}}\right)^{n_s+1}, \quad G_\ell^{(\text{EE})} \propto \left(\frac{\ell}{\ell_{\text{p}}}\right)^{n_s+1}, \quad G_\ell^{(\text{TE})} \propto \left(\frac{\ell}{\ell_{\text{p}}}\right)^{n_s} \quad (1.3)$$

where the notation \propto signifies that the corresponding quantity scales with the multipole in a given manner². When the scalar spectral index changes from the best-fit value (i.e.

²In Eq. (1.3) ℓ_{p} denotes the pivot multipole at which the initial conditions are customarily set. This scale is largely conventional and it will be hereby chosen to coincide with $\ell = 29$ which does correspond to the pivot wavenumber $k_{\text{p}} = 0.002 \text{ Mpc}^{-1}$.

$n_s = 0.963$) to a different value $G_\ell^{(\text{TT})}$ and $G_\ell^{(\text{EE})}$ will be modified according to Eq. (1.3). On the vertical axis of the plots reported in Fig. 1 the ratios $G_\ell^{(\text{TT})}(n_s = 0.963)/G_\ell^{(\text{TT})}(n_s = 1)$ and $G_\ell^{(\text{EE})}(n_s = 0.963)/G_\ell^{(\text{EE})}(n_s = 1)$ are computed numerically (full line) and analytically (as they emerge from Eq. (1.3)).

There are scaling relations involving, at once, different parameters. As it is known from elementary considerations, the height of the first peak in the acoustic oscillations of $G_\ell^{(\text{TT})}$ scales with first power the sound speed of the baryon photon fluid, which depends, in turn, upon the critical fraction of baryons; in formulae:

$$c_{\text{sb}}(z_*) = \frac{1}{\sqrt{3[1 + R_b(z_*)]}}, \quad R_b(z) = \frac{3\rho_b}{4\rho_\gamma} = 30.36\omega_b \left(\frac{10^3}{z_*}\right), \quad (1.4)$$

where $\omega_b = h_0^2\Omega_{b0}$ and z_* is the redshift of the last scattering. The examples can be multiplied by considering all the parameters of the Λ CDM scenario either alone or in some appropriate combinations. Instead of considering the dependence of the temperature and polarization anisotropies upon the various parameters listed at the right hand side of Eq. (1.2), it is often practical to consider a class of truly physical parameters emerging directly from the analysis of the various power spectra (see, e.g. [12, 13, 14, 15] and references therein). Concrete examples along this line are:

- the relative heights of the first three peaks in $G_\ell^{(\text{TT})}$;
- the positions of the peaks in all the observed angular power spectra (i.e. $G_\ell^{(\text{TT})}$, $G_\ell^{(\text{EE})}$ and $G_\ell^{(\text{TE})}$) their heights, their depths, their mutual distances;
- the numerical value of the acoustic multipole³;

and so on and so forth. The height of the first acoustic peak does not have a simple dependence upon the parameters of Eq. (1.2). Conversely, in terms of the quantities of Eq. (1.2), some power spectra exhibit rather contrived scaling properties which become instead manifest as a function of appropriate sets of derived variables which are accessible to direct observations. For instance, in the standard Λ CDM paradigm, the numerical values of the position of the anticorrelation peak in the TE power spectrum can be easily related to the position of the first Doppler peak in the TT power spectra; the height of the anticorrelation peak itself, however, does not have comparatively simple scaling with the parameters of Eq. (1.2).

The CMB observables can be indeed studied in terms of a set of so-called normal parameters whose distinctive feature is that their mutual correlation is (or at least should be) very small. One of the purposes of the present paper is to look for similar types of scaling relations but in a qualitatively different case, i.e. when the model contains, on top of Λ CDM

³The acoustic multipole is defined as $\ell_A = \pi D_A(z_*)/r_s(z_*)$ where $D_A(z_*)$ and $r_s(z_*)$ are, respectively, the comoving angular diameter distance and is the sound horizon at last scattering.

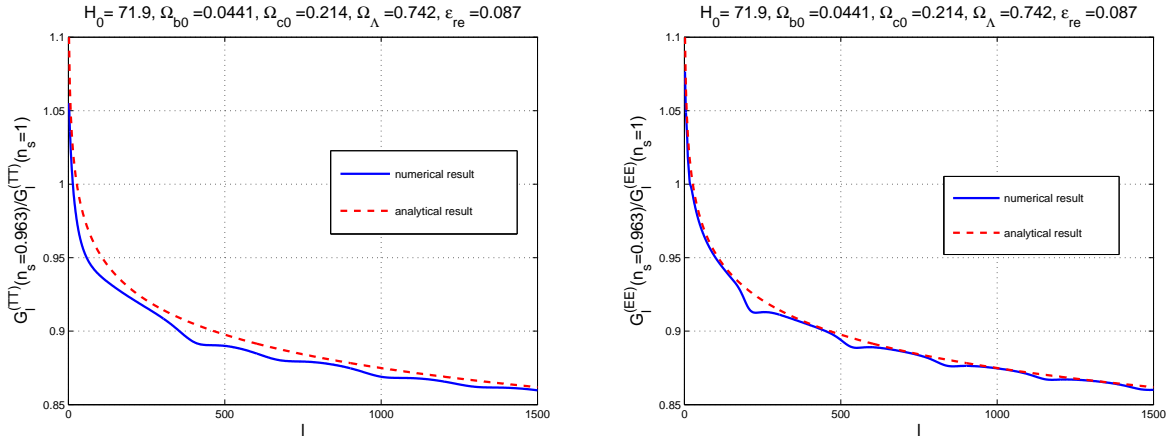


Figure 1: The usefulness of scaling relations is illustrated in a simplified situation involving the variation of the scalar spectral index from the best-fit value of the WMAP 5yr data alone (i.e. $n_s = 0.963$) to an exact Harrison-Zeldovich spectrum (i.e. $n_s = 1$).

parameters, also an ambient magnetic field. To be even more specific we wish to consider the situation where the Λ CDM paradigm includes also a magnetized background whose presence necessarily entails supplementary parameters. The minimal situation, in this respect, contemplates two new parameters, i.e. the magnetic spectral index n_B and the magnetic field amplitude B_L . In this case Eq. (1.2) becomes

$$G_\ell^{(XY)} = G_\ell^{(XY)}(n_B, B_L, n_s, \Omega_{b0}, \Omega_{c0}, \Omega_\Lambda, H_0, \epsilon_{re}). \quad (1.5)$$

To formulate in visual terms the main problem addressed in the present investigation, it is useful to look at Fig. 2 which, in some way, is the analog of Fig. 1 but in the case when large-scale magnetic fields are consistently included in the pre-decoupling physics. In the two plots at the left of Fig. 2 the TT and EE angular power spectra are presented in two cases, i.e. in the absence of an ambient magnetic field (dashed line in both plots) and in the case when a magnetic field modifies the initial conditions and the evolution of CMB anisotropies (full lines in both plots at the left). Just for illustrative purposes the magnetic spectral index and the comoving magnetic field amplitude have been chosen to be, respectively, $n_B = 1.5$ and $B_L = 20$ nG. Always in Fig. 2 (but in the two plots at the right) the TT and the EE angular power spectra have been divided by the corresponding power spectra but computed in the absence of magnetic fields. In other words, in the plots at the right the two curves stem from the ratio of the angular power spectra illustrated in the right plots of the same Fig. 2. Already at a qualitative level, the right plot of Fig. 2 shows interesting features like, for instance, different periodicities but similar growth rates with the multipole number. Is it possible to understand these as well as other features in analytic terms? This is one of the questions we ought to address. Another question could be: as in Fig. 1 the scaling properties can be used to infer the variation of the power spectra with the scalar spectral

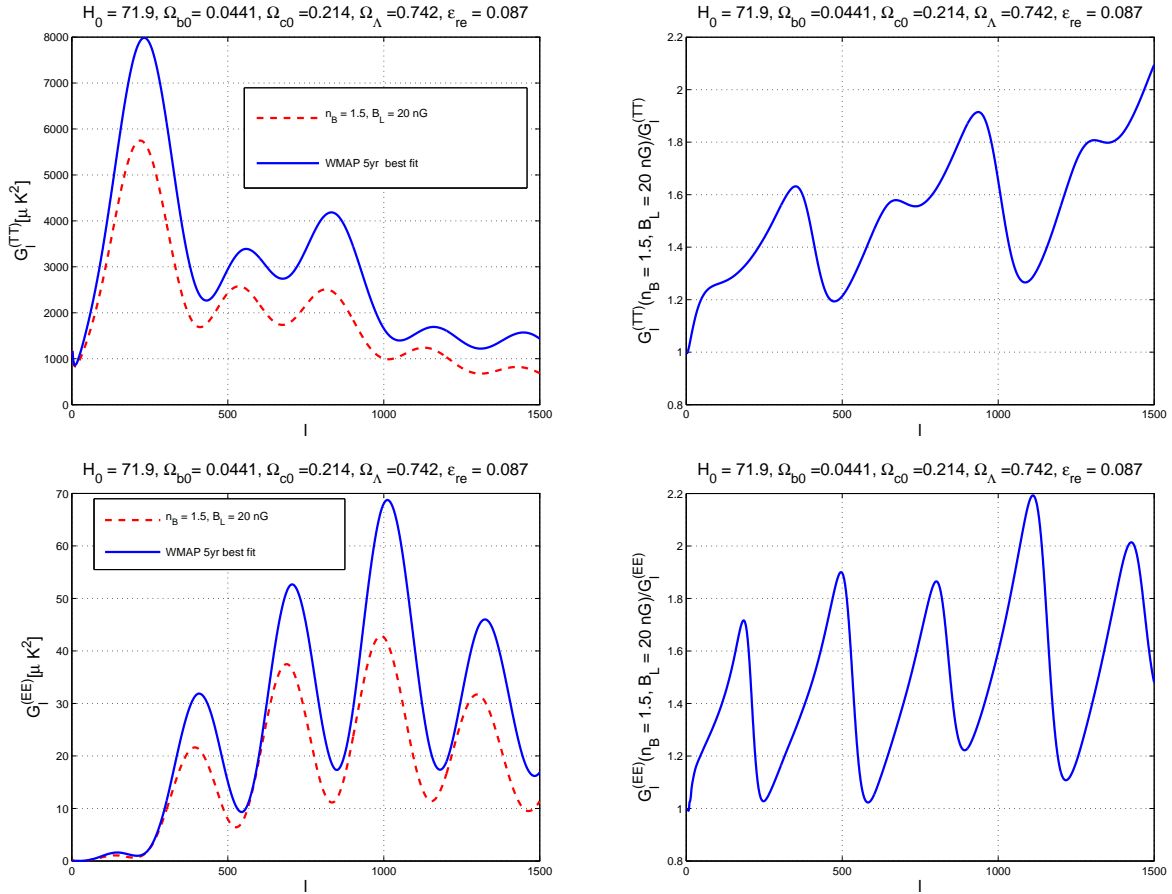


Figure 2: The temperature and polarization autocorrelation (plots at the left). In the plots at the right we report the ratios $G_\ell^{(XX)}(n_B \neq 0, B_L \neq 0)/G_\ell^{(XX)}$ with $X = T, E$. By definition $G_\ell^{(XX)} = G_\ell^{(XX)}(n_B = 0, B_L = 0)$ i.e. G_ℓ^{XX} denotes either the temperature or the polarization autocorrelations in the absence of ambient magnetic field.

index, can we do the same when large-scale magnetic fields are present? To achieve such a purpose it will prove useful to employ different approximations schemes which served as basic ingredients for developing the numerical techniques that led to the results of Fig. 2.

Before going through the plan of the investigation it is appropriate to swiftly remind the main motivations related to the study of the magnetized Universe (see, e.g. [16, 17] for dedicated reviews on the subject) which is basically the research program pursued here. Magnetic fields in gravitationally bound systems are a rather mundane feature of our Universe but one of the least understood especially when the typical correlation scale of the field is large as it happens, for instance, in the case of galaxies, clusters or even superclusters. Since the pioneering works of Alfvén and Fermi [18, 19, 20] (see also [21, 22]) large-scale magnetic fields have been the subject of numerous speculations whose detailed nature cannot be summarized here. The interested reader is referred to review articles such as [16] and to the

references of more recent publications [23, 24, 25, 26, 27]. It would be difficult to account for the detailed arguments leading to the different ideas which can eventually originate large-scale magnetism. Furthermore, as it will be argued below, the overall spirit of the present approach is more pragmatic; instead of dwelling on the rigor of the speculations leading to large-scale magnetism, it seems more urgent, on a physical ground, to decide which are the measurable effects of pre-decoupling magnetism. The latter quest is also experimentally better founded since the degree of rigor of a speculation is always rather complicated to assess and might strongly depend upon the theoretical prejudice of the authors.

The characteristics of the approaches discussed in this paper do not exclude the possibility of magnetizing the early history of the Universe [16] which is a rather intriguing subject of speculations dating back to the pioneering works of Zeldovich [28] and, independently, Harrison [29, 30] (see also [16] for further details). The early phases of the evolution of the Universe are often connected with an inflationary epoch ⁴ where, however, it seems to be rather difficult to produce large-scale magnetic fields in four-dimensional Friedmann-Robertson-Walker Universes. This impasse is related to the peculiar form of the evolution equations of Maxwell fields in curved backgrounds which are, technically, invariant under the Weyl rescaling of the geometry. To amplify gauge fields one might want to extend his model to higher-dimensional frameworks [31] or couple the kinetic term of the gauge fields to a spectator field [23]. Magnetogenesis models based on the dynamics of an appropriate spectator field delicately improve on the structure of conventional inflationary models and can be directly constrained by CMB data [23]. In spite of the specific model it seems relevant that the amplified gauge fields are Abelian. The only non-screened vector modes that are present at finite conductivity are the ones associated with the hypercharge field. The non-Abelian fields develop actually a mass and they are screened as the Universe thermalizes. After the electroweak phase transition the photon field remains unscreened with amplitude $\cos \theta_w \vec{\mathcal{Y}}$ where $\vec{\mathcal{Y}}$ is the hypercharge field and θ_w is the Weinberg's angle. While it is certainly interesting to speculate on the origin of large-scale magnetism prior to matter-radiation equality (i.e. for redshifts larger than, approximately, 3200) it is also rather urgent, as it will be argued in section 2, to scrutinize the CMB observables with the purpose of falsifying the statement that large-scale magnetic fields were indeed present around matter-radiation equality and, later, at the epoch of photon decoupling (i.e. for a typical redshift of the order of 1100).

Large-scale magnetic fields are a well defined object of experimental study since the pioneering contributions of Hiltner and Hall correctly interpreted in terms of a large-scale

⁴ Large-scale magnetic fields produced inside the Hubble radius after inflation will have a correlation scale bounded (from above) by the Hubble radius at the moment when some charge separation is produced (be it, for instance, the electroweak time). Since the Hubble radius, during radiation, evolves much faster than the correlation scale of the produced field, the typical scale over which the magnetic field is coherent today is much shorter than the Mpc, obliterating, in this way, the possibility of successfully reproducing the galactic magnetic field [16].

(interstellar) magnetic field by Davis and Greenstein [32]. For extended reviews on galactic magnetism see [33] and [34]. Large-scale magnetism is also a well established phenomenon in rich (i.e. Abell) clusters of galaxies [35] (see also [36, 37]) as well as, still with large uncertainties, in superclusters [38]. Magnetic fields in normal galaxies at high redshifts [39] could be already strong and this would be theoretically suggestive, in spite of the necessary caveats stemming from the large observational uncertainties (similar, in nature, to the ones experience while observing supercluster magnetism). Since we do observe large-scale for progressively larger redshifts it is natural to ask what happens at the photon decoupling especially because of the wealth of CMB data. In investigating such a class of phenomena the idea is to frame the least number of hypotheses on the subsequent evolution of large-scale magnetic fields so that we will take as starting point a faithful plasma description which is exactly the one employed in terrestrial laboratories [40, 41, 42, 43].

Having spelled out the general perspective of the present paper, its layout is, in short, the following. In section 2 the physics of the strongly and weakly interacting species at the epoch of photon decoupling will be briefly summarized with emphasis on the role of large-scale magnetic fields. Such a discussion will provide, in a reasonably self-contained perspective, all the equations which will be employed in the subsequent analysis. Section 3 treats the analytical methods employed in the line of sight solutions of the Boltzmann hierarchy, while, in section 4 the (magnetized) temperature and polarization anisotropies are computed in terms of a set of 8 basic integrals. Section 5 illustrates the comparison of analytical and numerical results while Section 6 deals with the analysis of the parameter space of magnetized CMB anisotropies. Section 7 contains the concluding considerations.

2 Strongly and weakly interacting species

Prior to decoupling the evolution of the plasma can be described in terms of charged and neutral species. Charged species interact directly with the ambient magnetic field whose effect, on the neutral species, is mediated by the relativistic fluctuations of the geometry. The separate role of the electrons and ions is often overlooked when the relativistic fluctuations of the geometry are consistently taken into account. The approach initially formulated in [44, 45] and developed in [46] is based on a rather conservative perspective: instead to doing a lot of effort to compute exotic phenomena triggered by large-scale magnetic fields, it is logically more urgent to compute in detail how large-scale magnetic fields affect CMB observables (see [47] for a more detailed formulation of such a research program). If large-scale magnetic fields gravitate and interact, simultaneously, with electrons and protons the most relevant effects on the temperature and polarization observables will be the one coming from the scalar modes of the geometry [44, 45, 46].

The scalar modes of the geometry admit two kinds of initial data which allow for the inclusion of large-scale magnetic fields, i.e. adiabatic initial conditions leading to the magnetized adiabatic mode (see [44, 45, 48]) and entropic initial conditions leading to various

magnetized isocurvature modes (see [49]). In what follows the main focus will be on the magnetized adiabatic mode. However, the same considerations developed here can be easily extended to the case of entropic initial conditions. In the case of adiabatic initial conditions the fluctuations of the spatial curvature are due to the fluctuations of the energy density while the fluctuations of the specific entropy are strictly vanishing at large scales. In the case of entropic initial conditions the curvature inhomogeneities are due to the fluctuations of the sound speed which are related, in turn, to the fluctuations of the specific entropy (see last part of section 2). Non-adiabatic initial conditions can be observationally constrained in different ways [50, 51, 52, 53, 54] and may lead, in the magnetized case, to interesting shape effects on the CMB observables. There are, of course, also different themes which involve the physics of large-scale magnetic fields in connection with CMB physics (see [47] for a dedicated review). For instance, large-scale (tangled) magnetic fields might have also specific effects related to the vector and tensor modes of the geometry (which are minute at large scales). These effects have been analyzed, at various levels of concreteness, in [55, 56, 57] (see also [58, 59] and compare them to [44, 45, 46, 49, 60]).

Depending upon their interaction rates, the constituents of the plasma can be classified into two groups: the strongly interacting species (such as the electrons, the protons and the photons) and the weakly interacting constituents (such as the CDM particles and the neutrinos). The difference between the two aforementioned categories resides in electromagnetic interaction which strongly affects the evolution of the electron-photon-ion system while it affects only indirectly the evolution of the weakly interacting species. The indirect effect of large-scale magnetic fields on the weakly interacting species comes from gravitational interactions: since large-scale magnetic fields gravitate, the relativistic fluctuations of the geometry are modified by their presence via the enforcement of the various constraints stemming from Einstein equations. There is a whole class of effects which are related to the high-frequency branch of the spectrum of plasma excitations [60, 61] which can be treated within the same framework described here (i.e. the magnetized adiabatic mode). In what follows, however, the focus will be on the scaling properties of the TT, EE and TE correlations since the angular power spectra of the B-mode polarization have been the subject of a separate study (see [60], second and third papers). It should be stressed that the values of the magnetic fields used in this paper are, sometimes, extreme, e.g. intensities of 10 nG are by far excluded both by direct limits stemming from the polarization observables [60, 61] and from the analysis of the peak structure of the TT correlations [62]. In [62] the WMAP 5yr data have been analyzed by including the effects of large-scale magnetic fields. In this perspective, for instance, the parameters reported in Fig. 2 are excluded. More specifically, the values⁵ $(n_B, B_L) = (2, 10\text{nG})$ are excluded, by the analysis of the TT and TE, to 95 % confidence level. At the same time, it is useful to illustrate the results in terms of these

⁵The magnetic field intensity and the magnetic spectral index are assigned as in [46, 48] (see also second and third paper of [60]). In the present context, B_L is the comoving amplitude of the field regularized over a typical scale $k_L = \text{Mpc}^{-1}$.

extreme values since, in this way, the visual impact is more pronounced and the scaling of the results with the parameters of the ambient magnetic field more evident.

2.1 Generalities

The simplest description of the pre-decoupling plasma in the presence of large-scale magnetic fields can be derived from the general pair of equations:

$$R_{\mu}^{\nu} - \frac{1}{2}\delta_{\mu}^{\nu}R = 8\pi GT_{\mu}^{\nu}, \quad (2.1)$$

$$\nabla_{\mu}F^{\mu\nu} = 4\pi j^{\nu}. \quad (2.2)$$

In Eq. (2.1) $R_{\mu\nu}$ is the Ricci tensor, R is the Ricci scalar and T_{μ}^{ν} is the total energy-momentum tensor of the system. In Eq. (2.2) $F^{\mu\nu}$ is the Maxwell field strength and j^{ν} is the total current of the system. Both the total energy momentum tensor and the total current must be covariantly conserved, i.e.

$$\nabla_{\mu}j^{\mu} = 0, \quad \nabla_{\mu}T^{\mu\nu} = 0. \quad (2.3)$$

In Eq. (2.3) ∇_{μ} denotes the covariant derivative. The total energy-momentum tensor is given by:

$$T^{\mu\nu} = T_{(e)}^{\mu\nu} + T_{(i)}^{\mu\nu} + T_{(\nu)}^{\mu\nu} + T_{(\gamma)}^{\mu\nu} + T_{(c)}^{\mu\nu} + T_{(\Lambda)}^{\mu\nu} + T_{(EM)}^{\mu\nu}, \quad (2.4)$$

where the subscripts denote, respectively, the contributions of electrons, ions, neutrinos, photons and CDM particles. More quantitatively the energy-momentum tensors of the different species are:

$$T_{(e)}^{\alpha\beta} = \rho_e u_{(e)}^{\alpha} u_{(e)}^{\beta}, \quad T_{(i)}^{\alpha\beta} = \rho_i u_{(i)}^{\alpha} u_{(i)}^{\beta}, \quad T_{(c)}^{\alpha\beta} = \rho_c u_{(c)}^{\alpha} u_{(c)}^{\beta} \quad (2.5)$$

$$T_{(\nu)}^{\alpha\beta} = \frac{4}{3}\rho_{\nu} u_{(\nu)}^{\alpha} u_{(\nu)}^{(\beta)} - \frac{\rho_{\nu}}{3}g^{\alpha\beta}, \quad T_{(\gamma)}^{\alpha\beta} = \frac{4}{3}\rho_{\gamma} u_{(\gamma)}^{\alpha} u_{(\gamma)}^{(\beta)} - \frac{\rho_{\gamma}}{3}g^{\alpha\beta}, \quad (2.6)$$

$$T_{(EM)}^{\alpha\beta} = \frac{1}{4\pi} \left[-F^{\alpha\mu} F_{\mu}^{\beta} + \frac{1}{4}g^{\alpha\beta} F_{\mu\nu} F^{\mu\nu} \right], \quad T_{\Lambda}^{\alpha\beta} = \rho_{\Lambda} g^{\alpha\beta}, \quad (2.7)$$

where $F_{0i} = -a^2 \mathcal{E}_i$ and $F_{ij} = -a^2 \epsilon_{ijk} \mathcal{B}^k$ are the components of the electromagnetic field strengths expressed, respectively, in terms of the electric and magnetic fields. In Eq. (2.6) the energy-momentum tensor of the neutrinos should also contain a contribution from the anisotropic stress which is, however, fully inhomogeneous and affects the evolution of the curvature perturbations rather than the evolution of the background metric. The total current of the system is due to electrons and ions, i.e.

$$j^{\mu} = e \tilde{n}_i u_{(i)}^{\mu} - e \tilde{n}_e u_{(e)}^{\mu},$$

$$g_{\mu\nu} u_{(i)}^{\mu} u_{(i)}^{\nu} = 1, \quad g_{\mu\nu} u_{(e)}^{\mu} u_{(e)}^{\nu} = 1, \quad (2.8)$$

where e denotes the electric charge⁶; \tilde{n}_e and \tilde{n}_i are the physical (as opposed to comoving) concentrations of the electrons and of the ions.

The evolution equations of the background geometry follow directly from Eq. (2.1) by recalling that, in the Λ CDM paradigm, the geometry is conformally flat (i.e. $g_{\mu\nu} = a^2\eta_{\mu\nu}$ where $\eta_{\mu\nu}$ is the Minkowski metric):

$$\mathcal{H}^2 = \frac{8\pi G}{3}a^2\rho_t, \quad (2.9)$$

$$\mathcal{H}^2 - \mathcal{H}' = 4\pi G a^2(p_t + \rho_t), \quad (2.10)$$

$$\rho_t' + 3\mathcal{H}(\rho_t + p_t) = 0. \quad (2.11)$$

In Eqs. (2.9), (2.10) and (2.11)

- the prime denotes a derivation with respect to the conformal time coordinate τ ;
- $\mathcal{H} = a'/a$ which also implies $\mathcal{H} = aH$ where $H = \dot{a}/a$ (where the overdot denotes a derivation with respect to the cosmic time coordinate t ; recall that $dt = a(\tau) d\tau$);
- finally the total energy density and the total pressure are:

$$\rho_t = \rho_e + \rho_i + \rho_\gamma + \rho_\nu + \rho_c + \rho_\Lambda, \quad (2.12)$$

$$p_t = \frac{\rho_\gamma}{3} + \frac{\rho_\nu}{3} - \rho_\Lambda. \quad (2.13)$$

For purposes of presentation we started directly from the covariantly conserved evolution of the energy-momentum tensor. It can be shown that this description is fully equivalent to a truncated Vlasov-Landau description [47, 48].

2.2 Strongly interacting species

The photons, the electrons and the ions interact electromagnetically and their velocities are tied together by the presence of scattering terms. At the same time photons, electrons and ions affect the evolution of the background geometry (i.e. Eqs. (2.9)–(2.11) and (2.12)–(2.13)) and of its relativistic inhomogeneities. From Eq. (2.2) the evolution of the Maxwell fields obeys

$$\vec{\nabla} \cdot \vec{E} = 4\pi e(n_i - n_e), \quad (2.14)$$

$$\vec{\nabla} \cdot \vec{B} = 0, \quad (2.15)$$

$$\vec{\nabla} \times \vec{E} = -\vec{B}', \quad (2.16)$$

$$\vec{\nabla} \times \vec{B} = 4\pi e(n_i \vec{v}_i - n_e \vec{v}_e) + \vec{E}', \quad (2.17)$$

⁶In this paper the units will be such that $e^2/(\hbar c) = 1/137$. Furthermore, as it is apparent from Eq. (2.2), in front of $F_{\alpha\beta}F^{\alpha\beta}$, in the action, there is a factor $1/(16\pi)$ which is reflected in the 4π of Eq. (2.2). Within these conventions and imposing the natural system of units $\hbar = c = 1$, $1 \text{ Gauss} = 6.9241 \times 10^{-20} \text{ GeV}^2$.

where the comoving concentrations and the comoving electromagnetic fields are:

$$n_i = a^3 \tilde{n}_i, \quad n_e = a^3 \tilde{n}_e, \quad \vec{E} = a^2 \vec{\mathcal{E}}, \quad \vec{B} = a^2 \vec{\mathcal{B}}. \quad (2.18)$$

The evolution equations of the electrons, of the ions and of the photons must include the relevant scattering terms governing their mutual momentum exchanges:

$$\vec{v}'_e + \mathcal{H} \vec{v}_e = -\frac{e}{m_e a} [\vec{E} + \vec{v}_e \times \vec{B}] - \vec{\nabla} \phi + \frac{4}{3} \frac{\rho_\gamma}{\rho_e} a \Gamma_{\gamma e} (\vec{v}_\gamma - \vec{v}_e) + a \Gamma_{ei} (\vec{v}_i - \vec{v}_e), \quad (2.19)$$

$$\vec{v}'_i + \mathcal{H} \vec{v}_i = \frac{e}{m_p a} [\vec{E} + \vec{v}_i \times \vec{B}] - \vec{\nabla} \phi + \frac{4}{3} \frac{\rho_\gamma}{\rho_i} a \Gamma_{\gamma i} (\vec{v}_\gamma - \vec{v}_i) + a \Gamma_{ei} \frac{\rho_e}{\rho_i} (\vec{v}_e - \vec{v}_i), \quad (2.20)$$

$$\vec{v}'_\gamma = -\frac{1}{4} \vec{\nabla} \delta_\gamma - \vec{\nabla} \phi + a \Gamma_{\gamma i} (\vec{v}_i - \vec{v}_\gamma) + a \Gamma_{\gamma e} (\vec{v}_e - \vec{v}_\gamma). \quad (2.21)$$

The relevant interaction rates between the different species appearing in Eqs. (2.19), (2.20) and (2.21) are given by

$$\Gamma_{\gamma e} = \tilde{n}_e \sigma_{e\gamma}, \quad \Gamma_{\gamma i} = \tilde{n}_i \sigma_{i\gamma}, \quad \sigma_{e\gamma} = \frac{8}{3} \pi \left(\frac{e^2}{m_e} \right)^2, \quad \sigma_{i\gamma} = \frac{8}{3} \pi \left(\frac{e^2}{m_i} \right)^2, \quad (2.22)$$

$$\Gamma_{ei} = \tilde{n}_e \sqrt{\frac{T}{m_e}} \sigma_{ei} = \Gamma_{ie}, \quad \sigma_{ei} = \frac{e^4}{T^2} \ln \Lambda_C, \quad \Lambda_C = \frac{3}{2e^3} \sqrt{\frac{T^3}{\tilde{n}_e \pi}}, \quad (2.23)$$

where T is the temperature and Λ_C is the Coulomb log [40, 41]. In Eqs. (2.19), (2.20) and (2.21) ϕ denotes one of the two longitudinal fluctuations of the geometry [63] whose explicit form is given by ⁷

$$\delta_s g_{00} = 2a^2 \phi, \quad \delta_s g_{ij} = 2a^2 \psi \delta_{ij}. \quad (2.24)$$

The density contrasts of the strongly interacting species evolve, respectively, as

$$\delta'_e = -\vec{\nabla} \cdot \vec{v}_e + 3\psi' - \frac{e}{m_e a} \vec{E} \cdot \vec{v}_e, \quad (2.25)$$

$$\delta'_i = -\vec{\nabla} \cdot \vec{v}_i + 3\psi' + \frac{e}{m_p a} \vec{E} \cdot \vec{v}_i, \quad (2.26)$$

$$\delta'_\gamma = 4\psi' - \frac{4}{3} \vec{\nabla} \cdot \vec{v}_\gamma. \quad (2.27)$$

Equations (2.19), (2.20) and (2.21) describe, together with Eqs. (2.25)–(2.27), a three-fluid system formed by photons, electrons and ions. At early times, i.e. well before photon decoupling, $\Gamma_{ei} \gg \Gamma_{\gamma e} \gg H$ and $\Gamma_{\gamma e} \gg \Gamma_{\gamma i}$ (since $m_p \gg m_e$). The three fluid system can therefore be described in terms of two effective fluids. The main equations of the system, in this regime, are therefore the appropriate generalization of the familiar magnetohydrodynamical reduction [40, 41, 42, 43] but in the case where the relativistic fluctuations of the geometry are consistently included in the original equations of the multicomponent plasma.

⁷In Eq. (2.24) and in what follows, $\delta_s(\dots)$ denotes the scalar fluctuation of the corresponding quantity.

By summing and subtracting Eqs. (2.19) and (2.20) the following pair of equations can be easily obtained, i.e.

$$\vec{v}'_b + \mathcal{H}\vec{v}_b = \frac{\vec{J} \times \vec{B}}{a^4 \rho_b} - \vec{\nabla} \phi + \frac{4}{3} \frac{\rho_\gamma}{\rho_b} a \Gamma_{\gamma e} (\vec{v}_\gamma - \vec{v}_b), \quad (2.28)$$

$$\vec{J} = \sigma(\vec{E} + \vec{v}_b \times \vec{B}), \quad (2.29)$$

where $\rho_b = (m_e + m_p)\tilde{n}_0$. To derive Eqs. (2.28) and (2.29) it should be borne in mind that the plasma is globally neutral, i.e. that $\tilde{n}_i = \tilde{n}_e$. From the evolution equations of the density contrasts (i.e. Eqs. (2.25) and (2.26)) it follows that

$$\delta'_b = -\vec{\nabla} \cdot \vec{v}_b + 3\psi' + \frac{\vec{J} \cdot \vec{E}}{a^4 \rho_b}, \quad (2.30)$$

where, by definition,

$$\delta_b = \frac{m_e}{m_p + m_e} \delta_e + \frac{m_p}{m_p + m_e} \delta_i, \quad \delta_b = \frac{\delta \rho_b}{\rho_b}, \quad \delta \rho_b = \delta \rho_e + \delta \rho_i. \quad (2.31)$$

Equations (2.28), (2.29) and (2.30) together with Eqs. (2.21) and (2.27) describe the baryon-photon fluid whose velocities (see Eqs. (2.21) and (2.28)) obey

$$\vec{v}'_b + \mathcal{H}\vec{v}_b = \frac{\vec{J} \times \vec{B}}{a^4 \rho_b} - \vec{\nabla} \phi + \frac{\epsilon'}{R_b} (\vec{v}_\gamma - \vec{v}_b), \quad (2.32)$$

$$\vec{v}'_\gamma = -\frac{1}{4} \vec{\nabla} \delta_\gamma - \vec{\nabla} \phi + \epsilon' (\vec{v}_e - \vec{v}_b), \quad (2.33)$$

where R_b is the baryon-to-photon ratio already introduced in Eq. (1.4) and where the differential optical depth $\epsilon' = a \Gamma_{\gamma e} = a \tilde{n}_0 x_e \sigma_{e\gamma}$ has been introduced.

The evolution equations for the photon-baryon system are the basis for the magnetohydrodynamical description of the problem and for the analysis of the initial conditions of the Einstein-Boltzmann hierarchy [44, 45, 46, 48]. The differential optical depth enters directly the visibility function which gives the probability that a photon is emitted between τ and $\tau + d\tau$:

$$\mathcal{K}(\tau) = \epsilon' e^{-\epsilon(\tau, \tau_0)}, \quad \epsilon(\tau, \tau_0) = \int_\tau^{\tau_0} a(\tau') \tilde{n}_0(\tau') \sigma_{\gamma e} d\tau'. \quad (2.34)$$

The visibility function which will be adopted for the analytic estimates can be approximated with a double Gaussian whose first peak arises around last scattering (i.e. for $\tau \simeq \tau_*$)

$$\mathcal{K}(\tau) = \mathcal{N}(\sigma_*) e^{-\frac{(\tau - \tau_*)^2}{2\sigma_*^2}}, \quad 0 < \tau < \tau_x, \quad (2.35)$$

where τ_x is an intermediate conformal time such that $\tau_x < \tau_{\text{re}}$ where τ_{re} is the reionization time. In Eq. (2.35), $\mathcal{N}(\sigma_*)$ is determined by requiring that the integral of $\mathcal{K}(\tau)$ over τ is normalized to 1. The WMAP data suggest a thickness (in redshift space) $\Delta z_* \simeq 195 \pm 2$ which

would imply that σ_* , in units of the (comoving) angular diameter distance to recombination, can be estimated as $\sigma_*/\tau_0 \simeq 1.43 \times 10^{-3}$. When $\tau_0 \gg \tau_*$ and $\tau_0 \gg \sigma_*$ the normalization appearing in Eq. (2.35) can be estimated as $\mathcal{N}(\sigma_*) \rightarrow \sigma_*^{-1} \sqrt{2/\pi}$. The second peak occurs for the reionization epoch. Also in this case the visibility function can be approximated with a Gaussian profile centered, this time, around τ_{re} . The specific form of the profile can be obtained from Eq. (2.35) by replacing (τ_*, σ_*) with $(\tau_{\text{rec}}, \sigma_{\text{rec}})$ and by taking into account that $z_{\text{re}} = 11 \pm 1.4$. The Gaussian (or double Gaussian) parametrization of the visibility has been used in several works (see, e.g. [64, 65] and also [66, 67]).

Prior to decoupling the system can be further simplified. The photon and the baryon velocities are quickly synchronized because of the hierarchy between the scattering rate and the Hubble rate. Thus, the evolution equations of the photon-baryon system effectively reduce to:

$$\delta'_\gamma = 4\psi' - \frac{4}{3}\vec{\nabla} \cdot \vec{v}_{\gamma\text{b}}, \quad (2.36)$$

$$\delta'_\text{b} = 3\psi' - \vec{\nabla} \cdot \vec{v}_{\gamma\text{b}} + \frac{\vec{J} \cdot \vec{E}}{a^4 \rho_\text{b}}, \quad (2.37)$$

$$\vec{v}'_{\gamma\text{b}} + \frac{\mathcal{H}R_\text{b}}{R_\text{b} + 1} \vec{v}_{\gamma\text{b}} - \frac{\eta}{\rho_\gamma(1 + R_\text{b})} \nabla^2 \vec{v}_{\gamma\text{b}} = -\frac{\vec{\nabla} \delta_\gamma}{4(1 + R_\text{b})} - \vec{\nabla} \phi + \frac{3}{4a^4 \rho_\gamma} \vec{J} \times \vec{B}. \quad (2.38)$$

In Eq. (2.38), the shear viscosity term $\eta = (4/15)\rho_\gamma \lambda_{\text{TH}}$ depends upon the photon mean free path λ_{TH} which is, in turn, inversely proportional to the differential optical depth.

2.3 Weakly interacting constituents

The effect of the ambient magnetic field on the weakly interacting species is mediated by the relativistic fluctuations of the geometry which are affected by the scalar modes of the electromagnetic background. The evolution of the CDM is given by

$$\delta'_\text{c} = 3\psi' - \vec{\nabla} \cdot \vec{v}_\text{c}, \quad \vec{v}'_\text{c} + \mathcal{H}\vec{v}_\text{c} = -\vec{\nabla} \phi. \quad (2.39)$$

The evolution equation of the neutrinos can be written instead as

$$\delta'_\nu = -\frac{4}{3}\vec{\nabla} \cdot \vec{v}_\nu + 4\psi', \quad (2.40)$$

$$\vec{v}'_\nu = \vec{\nabla} \sigma_\nu - \frac{1}{4}\vec{\nabla} \delta_\nu - \vec{\nabla} \phi, \quad (2.41)$$

$$\sigma'_\nu = \frac{4}{15}\vec{\nabla} \cdot \vec{v}_\nu. \quad (2.42)$$

In Eqs. (2.41) and (2.42) σ_ν is related to the neutrino anisotropic stress as $\partial_i \partial^j \tilde{\Pi}_j^i = (p_\nu + \rho_\nu) \nabla^2 \sigma_\nu$. The weakly interacting species are affected by the action of large-scale magnetic fields through the evolution of the fluctuations of the geometry which obey the (perturbed)

Einstein equations. The (00) and (0*i*) perturbed components of Eq. (2.1) are, in the gauge (2.24),

$$\nabla^2\psi - 3\mathcal{H}(\mathcal{H}\phi + \psi') = 4\pi Ga^2(\delta_s\rho_t + \delta_s\rho_B + \delta_s\rho_E), \quad (2.43)$$

$$\vec{\nabla}(\mathcal{H}\phi + \psi') + 4\pi Ga^2\left[(p_t + \rho_t)\vec{v}_t + \frac{\vec{E} \times \vec{B}}{4\pi a^4}\right] = 0. \quad (2.44)$$

The (*ij*) component of the perturbed Einstein equations can be broken, respectively, into a trace full and a trace less part:

$$\psi'' + \mathcal{H}(\phi' + 2\psi') + (\mathcal{H}^2 + 2\mathcal{H}')\phi + \frac{1}{3}\nabla^2(\phi - \psi) = 4\pi Ga^2[\delta_s p_t + \delta_s p_B + \delta_s p_E], \quad (2.45)$$

$$\partial^i\partial^j(\phi - \psi) - \frac{\delta^{ij}}{3}\nabla^2(\phi - \psi) = 8\pi Ga^2[\tilde{\Pi}^{ij} + \Pi_E^{ij} + \Pi_B^{ij}], \quad (2.46)$$

where $\delta_s\rho_t$ and $\delta_s p_t$ are the total fluctuations of the energy density and of the pressure while

$$\delta_s\rho_B = \frac{B^2}{8\pi a^4}, \quad \delta_s\rho_E = \frac{E^2}{8\pi a^4}, \quad \delta_s p_B = \frac{\delta_s\rho_B}{3}, \quad \delta_s p_E = \frac{\delta_s\rho_E}{3}, \quad (2.47)$$

$$\Pi_{Ej}^j = \frac{1}{4\pi a^4}\left[E_i E^j - \frac{\delta_i^j}{3}E^2\right], \quad \Pi_{Bj}^j = \frac{1}{4\pi a^4}\left[B_i B^j - \frac{\delta_i^j}{3}B^2\right], \quad (2.48)$$

where, as in Eq. (2.18), \vec{E} and \vec{B} denote the electromagnetic fields and, by definition, $\vec{B} = a^2\vec{\mathcal{B}}$ and $B^2 = B_i B^i$ while $E^2 = E_i E^i$. Furthermore, following the same notation employed for the neutrino anisotropic stress we shall denote

$$\partial_i\partial_j\Pi_E^{ij} = (p_\gamma + \rho_\gamma)\nabla^2\sigma_E, \quad \partial_i\partial_j\Pi_B^{ij} = (p_\gamma + \rho_\gamma)\nabla^2\sigma_B \quad (2.49)$$

2.4 The magnetized adiabatic mode

In what follows the attention will be focussed on the magnetized adiabatic mode for which all the possible entropic fluctuations vanish. This requirement implies that $\mathcal{S}_{ij} = -3(\zeta_i - \zeta_j)$ where the indices run over all the constituents of the plasma and where $\zeta_i = -\psi + \delta_i/[3(w_i + 1)]$. The vanishing of the entropy fluctuations vanish at large-scale (i. e. for $k\tau \ll 1$) implies that $\zeta_i = \zeta_j$, where, again the indices run over all the species of the plasma. The latter (gauge-invariant) condition reads off, in the gauge defined by Eq. (2.24) as

$$\delta_i = \frac{w_i + 1}{w_j + 1}\delta_j, \quad (2.50)$$

for any pair of constituents of the plasma.

To set the initial conditions of the Einstein-Boltzmann hierarchy the consistent solution of Eqs. (2.36)–(2.38), (2.39), (2.40)–(2.42), (2.43)–(2.44) and (2.45)–(2.46) should be found at the initial integration time τ_{initial} when the wavenumbers satisfy $k\tau_{\text{initial}} \ll 1$. As it is well

known the latter condition implies that the corresponding wavelengths are larger than the Hubble radius:

$$k\tau = \frac{k}{\mathcal{H}} = \frac{k}{aH} = \frac{k_{\text{phys}}}{H} \ll 1; \quad (2.51)$$

in Eq. (2.51), k is the comoving wavenumber and $k_{\text{phys}}(\tau) = k/a(\tau)$ is the physical wavenumber; furthermore $\mathcal{H} = aH$ where $H = \dot{a}/a$ and $\mathcal{H} = a'/a$ (see the comments after Eqs. (2.9), (2.10) and (2.11)). Equation (2.51) stipulates that the physical wavenumbers, at a given time, are always smaller than the Hubble rate implying, by definition, that the corresponding (physical) wavelengths are larger than the Hubble radius H^{-1} . Note that the first equality in Eq. (2.51) is exact in a pure radiation-dominated phase when $\mathcal{H} = \tau^{-1}$. In the realistic situation, however, the scale factor interpolates between the radiation-dominated and the matter-dominated epochs and $\mathcal{H} = (2/\tau_1)\sqrt{\alpha + 1}/\alpha$ where $\alpha = a/a_{\text{eq}} = [(\tau/\tau_1)^2 + 2(\tau/\tau_1)]$ (see also the discussion around Eqs. (3.11) and (3.12)).

If the condition (2.51) holds, then it is also true that $k/\sigma \ll k/\mathcal{H}$ where $\sigma = \sigma_c a$ is the conductivity. Indeed recall that

$$\sigma = \frac{T}{\alpha_{\text{em}}} \left(\frac{T}{m_e a} \right)^{1/2}, \quad H = \sqrt{\frac{4\pi^3 g_\rho}{45}} \frac{T_{\text{phys}}^2}{M_{\text{P}}}, \quad (2.52)$$

where $T = aT_{\text{phys}}$, g_ρ is the effective number of relativistic degrees of freedom and $M_{\text{P}} = 1/\sqrt{G} \simeq 1.22 \times 10^{19}$ GeV. Then we can write, in the case of a cold plasma,

$$\frac{k}{\sigma} = \alpha_{\text{em}} \frac{k_{\text{phys}}}{T_{\text{phys}}} \sqrt{\frac{m_e}{T_{\text{phys}}}} \equiv \alpha_{\text{em}} \left(\frac{k_{\text{phys}}}{H} \right) \left(\frac{4\pi^3 g_\rho}{45} \right)^{1/2} \left(\frac{m_e}{T_{\text{phys}}} \right)^{1/2} \left(\frac{T_{\text{phys}}}{M_{\text{P}}} \right). \quad (2.53)$$

According to Eq. (2.53), for $T_{\text{phys}} < \text{MeV}$, $k/\sigma \ll 1$ provided $k_{\text{phys}}/H \ll 1$. Equation (2.53) shows also that the condition $k/\sigma < 1$ holds also for wavelengths which are shorter than the Hubble (i.e. $k_{\text{phys}} > H$) since $T_{\text{phys}}/M_{\text{P}}$ is a really minute number (of the order of 10^{-28} for temperatures in the eV range).

The approximation scheme defined by Eqs. (2.51), (2.52) and (2.53) allows for a consistent solution of Eqs. (2.36)–(2.38), (2.39), (2.40)–(2.42), (2.43)–(2.44) and (2.45)–(2.46); the explicit form of the magnetized adiabatic mode can then be written as:

$$\begin{aligned} \phi(k) &= -\frac{10 \mathcal{R}_*(k)}{4R_\nu + 15} - 2 \frac{R_\gamma \{4\sigma_{\text{B}}(k) - R_\nu[\Omega_{\text{B}}(k) + \Omega_{\text{E}}(k)]\}}{4R_\nu + 15}, \\ \psi(k) &= \left(1 + \frac{2}{5} R_\nu\right) \phi(k) + \frac{R_\gamma}{5} \{4[\sigma_{\text{B}}(k) + \sigma_{\text{E}}(k)] - R_\nu[\Omega_{\text{B}}(k) + \Omega_{\text{E}}(k)]\}, \\ \delta_\gamma(k, \tau) &= -2\phi(k) - R_\gamma[\Omega_{\text{B}}(k) + \Omega_{\text{E}}(k)], \\ \delta_\nu(k) &= -2\phi(k) - R_\gamma[\Omega_{\text{B}}(k) + \Omega_{\text{E}}(k)], \\ \delta_{\text{c}}(k) &= -\frac{3}{2}\phi(k) - \frac{3}{4}R_\gamma[\Omega_{\text{B}}(k) + \Omega_{\text{E}}(k)], \\ \delta_{\text{b}}(k) &= -\frac{3}{2}\phi(k) - \frac{3}{4}R_\gamma[\Omega_{\text{B}}(k) + \Omega_{\text{E}}(k)], \end{aligned}$$

$$\begin{aligned}
\sigma_\nu(k, \tau) &= -\frac{R_\gamma}{R_\nu}[\sigma_B(k) + \sigma_E(k)] + \frac{k^2\tau^2}{6R_\nu}[\psi(k) - \phi(k)], \\
\theta_{\gamma b}(k, \tau) &= \frac{k^2\tau}{2}\left[\phi(k) + \frac{R_\nu}{2}\Omega_B(k) - \frac{R_\gamma}{2}\Omega_E(k) - 2\sigma_B(k)\right], \\
\theta_\nu(k, \tau) &= \frac{k^2\tau}{2}\left[\phi(k) - \frac{R_\gamma\Omega_B(k)}{2} + 2\frac{R_\gamma}{R_\nu}(\sigma_B(k) + \sigma_E(k))\right], \\
\theta_c(k, \tau) &= \frac{k^2\tau}{2}\phi(k),
\end{aligned} \tag{2.54}$$

where $\mathcal{R}_*(k)$ is the curvature perturbation on comoving orthogonal hypersurfaces,

$$\mathcal{R}_*(k) = -\psi - \frac{\mathcal{H}(\mathcal{H}\phi + \psi')}{\mathcal{H}^2 - \mathcal{H}'} \simeq -\psi(k) - \frac{\phi(k)}{2}. \tag{2.55}$$

For notational convenience, in Eq. (2.54), $R_\gamma = 1 - R_\nu$ denotes the photon fraction in the radiation plasma and R_ν is given, by definition, as

$$R_\nu = \frac{\rho_\nu}{\rho_\gamma + \rho_\nu} = \frac{3 \times (7/8) \times (4/11)^{4/3}}{1 + 3 \times (7/8) \times (4/11)^{4/3}} = 0.4052, \tag{2.56}$$

where 3 counts the degrees of freedom associated with the massless neutrino families, (7/8) arises because neutrinos follow the Fermi-Dirac statistics; the factor $(4/11)^{4/3}$ stems from the relative reduction of the neutrino (kinetic) temperature (in comparison with the photon temperature) after weak interactions fall out of thermal equilibrium.

In Eq. (2.54) the following dimensionless quantities have also been introduced:

$$\Omega_E = \frac{\delta_s \rho_E}{\rho_\gamma}, \quad \Omega_B = \frac{\delta_s \rho_B}{\rho_\gamma}; \tag{2.57}$$

see also Eqs. (2.47) for a definition of $\delta_s \rho_E$ and $\delta_s \rho_B$; the quantities σ_E and σ_B have been already introduced in Eq. (2.49). It is finally useful to recall a pair of useful vector identities which connect σ_E and σ_B to Ω_E and Ω_B , i.e.

$$\nabla^2 \sigma_E = \frac{\nabla^2 \Omega_E}{4} + \frac{3}{16\pi\rho_\gamma a^4} \{ \vec{\nabla} \cdot [(\vec{\nabla} \times \vec{E}) \times \vec{E}] - 4\pi \vec{E} \cdot \vec{\nabla} \rho_q \}, \tag{2.58}$$

$$\nabla^2 \sigma_B = \frac{\nabla^2 \Omega_B}{4} + \frac{R_b}{a^4 \rho_b} \vec{\nabla} \cdot [\vec{J} \times \vec{B}], \tag{2.59}$$

where $\rho_q = e(n_i - n_e)$; $\vec{J} = \vec{\nabla} \times \vec{B}/(4\pi)$ is the total current in the one-fluid limit; R_b (see Eq. (1.4)) is the baryon-to-photon ratio.

Because of Eqs. (2.52)–(2.53), the contribution of the electric field fluctuations to the initial conditions turns out to be almost always negligible. At the same time it is interesting to consider, in some detail, the transient regime where some putative electric field dies off thanks to the large values of the conductivity. In the latter case Eqs. (2.54) and (2.55) allow for the inclusion of the electric field spectra in the initial conditions of the Einstein-Boltzmann hierarchy. This possibility will not be considered here but will be separately discussed.

2.5 Line of sight solution of the Boltzmann hierarchy

The temperature and polarization power spectra are, by definition,

$$C_\ell^{(\text{TT})} = \frac{1}{2\ell + 1} \sum_m \langle a_{\ell m}^{(\text{T})*} a_{\ell m}^{(\text{T})} \rangle, \quad (2.60)$$

$$C_\ell^{(\text{EE})} = \frac{1}{2\ell + 1} \sum_m \langle a_{\ell m}^{(\text{E})*} a_{\ell m}^{(\text{E})} \rangle, \quad (2.61)$$

$$C_\ell^{(\text{TE})} = \frac{1}{2\ell + 1} \sum_m \langle a_{\ell m}^{(\text{T})*} a_{\ell m}^{(\text{E})} \rangle. \quad (2.62)$$

In terms of the intensity and polarization fluctuations in real space (i.e. $\Delta_{\text{I}}(\hat{n}, \tau)$ and $\Delta_{\text{E}}(\hat{n}, \tau)$), the coefficients $a_{\ell m}^{(\text{T})}$ and $a_{\ell m}^{(\text{E})}$ are:

$$\begin{aligned} a_{\ell m}^{(\text{T})} &= \int d\hat{n} Y_{\ell m}^*(\hat{n}) \Delta_{\text{I}}(\hat{n}, \tau), \\ a_{\ell m}^{(\text{E})} &= N_\ell \int d\hat{n} Y_{\ell m}^*(\hat{n}) \Delta_{\text{E}}(\hat{n}, \tau), \end{aligned} \quad (2.63)$$

where \hat{n} denotes the direction of propagation of the radiation and $N_\ell = \sqrt{(\ell - 2)!/(\ell + 2)!}$. The (real space) E-mode fluctuation is defined as [70, 71] (see also [60, 72]):

$$\Delta_{\text{E}}(\hat{n}, \tau) = -\frac{1}{2} \{ K_-^{(1)}(\hat{n}) [K_-^{(2)}(\hat{n}) \Delta_+(\hat{n}, \tau)] + K_+^{(-1)}(\hat{n}) [K_+^{(-2)}(\hat{n}) \Delta_-(\hat{n}, \tau)] \}, \quad (2.64)$$

where $\Delta_\pm(\hat{n}, \tau) = \Delta_{\text{Q}}(\hat{n}, \tau) \pm i \Delta_{\text{U}}(\hat{n}, \tau)$ and where $K_\pm^s(\hat{n})$ are a pair of differential operators which can either raise or lower the spin-weight of a given function:

$$K_\pm^s(\hat{n}) = -(\sin \vartheta)^{\pm s} \left[\partial_\vartheta \pm \frac{i}{\sin \vartheta} \partial_\varphi \right] (\sin \vartheta)^{\mp s}. \quad (2.65)$$

The known advantage of dealing directly with the E-mode polarization (rather than with the Stokes parameters) is that $\Delta_{\text{E}}(\hat{n}, \tau)$ is a scalar (i.e. a function of spin-weight 0 [71]) for rotations around the direction of propagation of the radiation field. In this sense $\Delta_{\text{E}}(\hat{n}, \tau)$ is fully analog to $\Delta_{\text{I}}(\hat{n}, \tau)$, i.e. the brightness perturbation of the intensity of the radiation field which is, of course, a function of spin-weight 0. Defining the projection of the Fourier mode in the direction of the photon momentum as $\mu = \cos \vartheta$, the evolution of the intensity of the radiation field reads (in Fourier space):

$$\Delta_{\text{I}}' + (ik\mu + \epsilon') \Delta_{\text{I}} = \tilde{S}_{\text{I}}(k, \mu, \tau), \quad (2.66)$$

$$v_{\text{b}}' + \mathcal{H}v_{\text{b}} = \tilde{S}_{v_{\text{b}}}(k, \tau), \quad (2.67)$$

where

$$S_{\text{P}}(k, \tau) = \Delta_{\text{I}2} + \Delta_{\text{P}0} + \Delta_{\text{P}2} \quad (2.68)$$

$$\tilde{S}_{\text{I}}(k, \mu, \tau) = -ik\mu\phi + \psi' + \epsilon' \left[\Delta_{\text{I}0} + \mu v_{\text{b}} - \frac{(3\mu^2 - 1)}{4} S_{\text{P}}(k, \tau) \right], \quad (2.69)$$

$$\tilde{S}_{v_{\text{b}}}(k, \tau) = -\frac{\epsilon'}{R_{\text{b}}} (3i\Delta_{\text{I}1} + v_{\text{b}}) - ik \frac{\Omega_{\text{B}} - 4\sigma_{\text{B}}}{4R_{\text{b}}}. \quad (2.70)$$

Equation (2.67) is the Fourier space version of Eq. (2.32) and v_b is the divergence-full part \vec{v}_b . The Fourier transform of the intensity and of the E-mode polarization is defined, within the present conventions, as

$$\Delta_I(\hat{n}, \tau) = \frac{1}{(2\pi)^{3/2}} \int d^3k \Delta_I(k, \mu, \tau), \quad \Delta_E(\hat{n}, \tau) = \frac{1}{(2\pi)^{3/2}} \int d^3k \Delta_E(k, \mu, \tau). \quad (2.71)$$

From Eqs. (2.64)–(2.65) the explicit form of the E-mode polarization can be written:

$$\Delta_E(\hat{n}, \tau) = - \left\{ (1 - \mu^2) \Delta_Q'' - 4\mu \Delta_Q' - 2\Delta_Q - \frac{\partial_\varphi^2 \Delta_Q}{1 - \mu^2} - 2 \left[\partial_\varphi \Delta_U' - \frac{\mu}{1 - \mu^2} \partial_\varphi \Delta_U \right] \right\}. \quad (2.72)$$

In the case of the magnetized adiabatic mode Δ_U and Δ_Q do not have azimuthal dependence. Furthermore a B-mode polarization is only generated thanks to Faraday mixing which has been investigated analytically elsewhere [60, 61] and will not be repeated here. The total polarization degree coincides with the contribution of Δ_Q , i.e. $\Delta_Q(\hat{n}, \tau) = \Delta_P(\hat{n}, \tau)$. It follows from Eq. (2.72) that, in Fourier space, the E-mode polarization is

$$\Delta_E(k, \mu, \tau) = -\partial_\mu^2 [(1 - \mu^2) \Delta_P(k, \mu, \tau)], \quad (2.73)$$

where Δ_P obeys

$$\Delta_P' + (ik\mu + \epsilon') \Delta_P = \tilde{S}_P(k, \mu, \tau), \quad \tilde{S}_P(k, \mu, \tau) = \frac{3}{4} (1 - \mu^2) S_P(k, \tau). \quad (2.74)$$

Using line of sight integration the formal solution of Eqs. (2.66) and (2.74) can be formally written as [73, 74]:

$$\Delta_I(k, \mu, \tau_0) = \int_0^{\tau_0} e^{ik\mu(\tau-\tau_0)} e^{-\epsilon(\tau, \tau_0)} \tilde{S}_I(k, \mu, \tau) d\tau, \quad (2.75)$$

$$\Delta_P(k, \mu, \tau_0) = \int_0^{\tau_0} e^{ik\mu(\tau-\tau_0)} e^{-\epsilon(\tau, \tau_0)} \tilde{S}_P(k, \mu, \tau) d\tau. \quad (2.76)$$

The solution expressed by Eqs. (2.75) and (2.76) assumes, implicitly, that the source terms can be independently evaluated either numerically or analytically. The approximation of tight Coulomb coupling will now be consistently used. The large-scale magnetic fields will then affect electrons and protons whose evolution can be determined in the appropriate one-fluid limit. It should be stressed that the approach discussed here is very similar, in spirit, to the various semi-analytic techniques which have been employed (in the absence of large-scale magnetic fields) by various authors [75, 76, 77] starting with the pioneering work of Peebles and Yu [78].

3 Temperature and polarization anisotropies

Assuming tight coupling between photons, electrons and baryons, the evolution of the monopole and of the dipole of the brightness perturbations determine the evolution of the

source term in the temperature and polarization anisotropies (i.e. Eqs. (2.66)–(2.67) and (2.74)). The monopole and the dipole obey, in Fourier space, the following pair of equations

$$(\psi - \Delta_{\text{I}0})' = k\Delta_{\text{I}1}, \quad (3.1)$$

$$[(R_{\text{b}} + 1)\Delta_{\text{I}1}]' + 2\frac{k^2}{k_{\text{D}}^2}(R_{\text{b}} + 1)\Delta_{\text{I}1} = \frac{k}{3}\Delta_{\text{I}0} + \frac{k(R_{\text{b}} + 1)}{3}\phi + \frac{k(\Omega_{\text{B}} - 4\sigma_{\text{B}})}{12}, \quad (3.2)$$

where R_{b} has been already introduced in Eq. (1.4) and where k_{D} is the wave-number corresponding to diffusive damping, i.e. the wave-number at which diffusive effects start being important. To lowest-order in the photon-baryon coupling the diffusive damping is simply proportional to the shear viscosity coefficient η which has been already introduced in Eq. (2.38). More precisely, to lowest order in the tight-coupling, $k_{\text{D}}^{-2} = \eta/[\rho_{\gamma}(1 + R_{\text{b}})]$ where η has been defined right after Eq. (2.38) and is proportional to the photon mean free path. The estimates based on shear viscosity can be improved by going to higher order in the tight-coupling expansion and by further refining the estimates depending upon the explicit values of the Λ CDM parameters. In particular, for typical values of the parameters close to the best-fit provided by the Λ CDM model the values of k_{D} and ℓ_{D} (i.e. the diffusive multipole) can be estimated as

$$\ell_{\text{D}} = k_{\text{D}} D_{\text{A}}(z_*) = \frac{2240 d_{\text{A}}(z_*)}{\sqrt{\sqrt{r_{\text{R}*} + 1} - \sqrt{r_{\text{R}*}}}} \left(\frac{z_*}{10^3}\right)^{5/4} \omega_{\text{b}}^{0.24} \omega_{\text{M}}^{-0.11}. \quad (3.3)$$

The (comoving) angular diameter distance at z_* has been rescaled, in Eq. (3.3) as

$$D_{\text{A}}(z_*) = \frac{2}{\sqrt{\Omega_{\text{M}0} H_0}} d_{\text{A}}(z_*). \quad (3.4)$$

Furthermore, always in Eq. (3.3) $r_{\text{R}*}$ is the ratio of the radiation and matter energy densities at z_* , i.e.

$$r_{\text{R}*} = \frac{\rho_{\text{R}}(z_*)}{\rho_{\text{M}}(z_*)} = \frac{a_{\text{eq}}}{a_*} = 4.15 \times 10^{-2} \omega_{\text{M}}^{-1} \left(\frac{z_*}{10^3}\right). \quad (3.5)$$

where, following the customary notation, $\omega_{\text{M}} = h_0^2 \Omega_{\text{M}0}$. The numerical content of Eqs. (3.3)–(3.5) is fully specified in terms of z_* whose explicit form can be written as

$$z_* = 1048[1 + (1.24 \times 10^{-3}) \omega_{\text{b}}^{-0.738}][1 + g_1 \omega_{\text{M}}^{g_2}], \quad (3.6)$$

$$g_1 = \frac{0.0783 \omega_{\text{b}}^{-0.238}}{[1 + 39.5 \omega_{\text{b}}^{0.763}]}, \quad g_2 = \frac{0.560}{1 + 21.1 \omega_{\text{b}}^{1.81}}. \quad (3.7)$$

Equations (3.6)–(3.7) imply $z_* = 1090.5$ in excellent agreement with the estimate of [1, 2, 3], i.e. $z_* = 1090.51 \pm 0.95$. The evolution of the monopole and of the dipole can be determined from the WKB solution of Eqs. (3.1) and (3.2), i.e.

$$\Delta_{\text{I}0}(k, \tau) + \phi(k, \tau) = \mathcal{L}(k, \tau) + \sqrt{c_{\text{sb}}} \mathcal{M}(k, \tau) \cos[kr_{\text{s}}(\tau)] e^{-\frac{k^2}{k_{\text{D}}^2}}, \quad (3.8)$$

$$\Delta_{\text{I}1}(k, \tau) = c_{\text{sb}}^{3/2} \mathcal{M}(k, \tau) \sin[kr_{\text{s}}(\tau)] e^{-\frac{k^2}{k_{\text{D}}^2}}, \quad (3.9)$$

where $\mathcal{L}(k, \tau)$ and $\mathcal{M}(k, \tau)$ are fixed once the initial conditions of the Einstein-Boltzmann hierarchy are specified. In what follows, as already mentioned, the initial conditions shall correspond to the magnetized adiabatic mode. In Eqs. (3.8) and (3.9) $r_s(\tau)$, is the sound horizon

$$r_s(\tau_*) = \int_0^{\tau_*} d\tau c_{\text{sb}}(\tau) = \int_0^{\tau_*} \frac{d\tau}{\sqrt{3[R_b(\tau) + 1]}}, \quad (3.10)$$

whose explicit form will be determined as a function of z_* . The explicit solution of Eqs. (2.9), (2.10) and (2.11) for the matter radiation transition implies that $a(x) = a_{\text{eq}}[x^2 + 2x]$ with $x = \tau/\tau_1$. This also means that:

$$\left(\frac{\tau_*}{\tau_1} + 1\right) = \sqrt{1 + \frac{a_*}{a_{\text{eq}}}} = \sqrt{\frac{1 + r_{\text{R}*}}{r_{\text{R}*}}}. \quad (3.11)$$

where $\tau_1 = 2\sqrt{(a_{\text{eq}}/\Omega_{\text{M}0})}/H_0$. By definition of baryon-to-photons ratio (see, e.g., Eq. (1.4)) we have that $R_b(x) = R_{\text{b}*}r_{\text{R}*}(x^2 + 2x)$. Thus, defining Eq. $y = x + 1$, Eq. (3.10) becomes easily

$$\begin{aligned} r_s(\tau_*) &= \frac{\tau_1}{\sqrt{3}} \int_0^{\tau_*/\tau_1} \frac{dx}{\sqrt{R_{\text{b}*}r_{\text{R}*}(x^2 + 2x) + 1}} \\ &= \frac{\tau_1}{\sqrt{3} R_{\text{b}*}r_{\text{R}*}} \int_1^{(\tau_*/\tau_1)+1} \frac{dy}{\sqrt{y^2 + y_0^2}}, \quad y_0 = \sqrt{\frac{1 - R_{\text{b}*}r_{\text{R}*}}{R_{\text{b}*}r_{\text{R}*}}}, \end{aligned} \quad (3.12)$$

which can be integrated via a further change of variables (i.e. $y = y_0 \sinh w$); the result is:

$$r_s(\tau_*) = \frac{\tau_1}{\sqrt{3} R_{\text{b}*}r_{\text{R}*}} \left\{ \operatorname{arcsinh} \left[\frac{(\tau_*/\tau_1) + 1}{y_0} \right] - \left[\frac{1}{y_0} \right] \right\}. \quad (3.13)$$

Since, by definition, $\operatorname{arcsinh}(\alpha) = \ln[\alpha + \sqrt{\alpha^2 + 1}]$ and τ_1 is given after Eq. (3.11) the sound horizon at τ_* is given by:

$$r_s(\tau_*) = \frac{2}{H_0} \frac{1}{\sqrt{\Omega_{\text{M}0}}} \frac{1}{\sqrt{3R_{\text{b}*}(z_* + 1)}} \ln \left[\frac{\sqrt{1 + R_{\text{b}*}} + \sqrt{R_{\text{b}*}}\sqrt{1 + r_{\text{R}*}}}{1 + \sqrt{r_{\text{R}*} R_{\text{b}*}}} \right]. \quad (3.14)$$

Having determined the monopole and the dipole by solving Eqs. (3.1) and (3.2) the polarization observables depend chiefly upon the value of the dipole as it arises to lowest order in the tight-coupling expansion. However, as it was already observed long ago [73], the first-order tight-coupling estimate is not satisfactory from the numerical point of view and must be improved. Following this logic, Eqs. (2.66) and (2.74) imply the following relations between the multipoles of the intensity and polarization brightness perturbations:

$$\Delta'_{\text{P}0} - \frac{\epsilon'}{2} [\Delta_{\text{P}2} + \Delta_{\text{I}2} - \Delta_{\text{P}0}] = -k\Delta_{\text{P}1}, \quad (3.15)$$

$$\Delta'_{\text{I}2} + \epsilon' \left[\frac{9}{10} \Delta_{\text{I}2} - \frac{1}{10} (\Delta_{\text{P}0} + \Delta_{\text{P}2}) \right] = -\frac{3}{5} k \Delta_{\text{I}3} + \frac{2}{5} k \Delta_{\text{I}1}, \quad (3.16)$$

$$\Delta'_{\text{P}2} + \epsilon' \left[\frac{9}{10} \Delta_{\text{P}2} - \frac{1}{10} (\Delta_{\text{P}0} + \Delta_{\text{I}2}) \right] = -\frac{3}{5} k \Delta_{\text{P}3} + \frac{2}{5} k \Delta_{\text{P}1}. \quad (3.17)$$

Summing up Eqs. (3.15), (3.16) and (3.17) and recalling that, by definition, $S_P = (\Delta_{I2} + \Delta_{P0} + \Delta_{P2})$, Eqs. (3.15)–(3.17) imply

$$S'_P + \frac{3}{10}\epsilon' S_P = k \left[\frac{2}{5}\Delta_{I1} - \frac{3}{5}(\Delta_{P1} + \Delta_{P3} + \Delta_{I3}) \right]. \quad (3.18)$$

The result of the solution of Eq. (3.18) turns out to be more accurate than the lowest order tight-coupling result. Indeed, neglecting Δ_{P1} , Δ_{P3} and Δ_{I3} (which are all smaller than Δ_{I1}) Eq. (3.18) can be formally integrated:

$$S_P(k, \tau) = \frac{2}{5}k e^{3\epsilon(\tau, \tau_0)/10} \int_0^\tau d\tau' \bar{\Delta}_{I1}(k, \tau') e^{-3\epsilon(\tau', \tau_0)/10}, \quad (3.19)$$

which also implies that

$$\Delta_P(k, \mu, \tau_0) = -0.515 (k \sigma_*) (1 - \mu^2) e^{ik\mu(\tau_* - \tau_0)} \bar{\Delta}_{I1}(k, \tau_*). \quad (3.20)$$

The coefficients $a_{\ell m}^{(T)}$ and $a_{\ell m}^{(E)}$ can be determined in terms of Eqs. (3.8)–(3.9) and (3.20) following the standard techniques. More specifically the coefficient $a_{\ell m}^{(T)}$ can be expressed as:

$$a_{\ell m}^{(T)} = \frac{\sqrt{4\pi}}{(2\pi)^{3/2}} (-i)^\ell \sqrt{2\ell + 1} \int d^3k e^{-\frac{k^2}{k_t^2}} \left[(\Delta_{I0} + \phi) j_\ell(x) + 3\Delta_{I1} \left(\frac{dj_\ell}{dx} \right) \right], \quad (3.21)$$

where $x = k(\tau_0 - \tau_*)$ and where $j_\ell(x)$ are the spherical Bessel functions [68, 69] of argument x . In Eq. (3.21) $k_t = \sqrt{3}/\sigma_*$ arises from the integration over τ of the Gaussian visibility function. The coefficient $a_{\ell m}^{(E)}$ turns out to be:

$$a_{\ell m}^{(E)} = \frac{3}{4} \frac{(-i)^\ell}{(2\pi)^{3/2}} \sqrt{\frac{(\ell - 2)!}{(\ell + 2)!}} \sqrt{4\pi} \sqrt{2\ell + 1} \int d^3k x^2 [(1 + \partial_x^2)^2] j_\ell(x) \int_0^{\tau_0} \mathcal{K}(\tau) S_P(k, \tau) d\tau. \quad (3.22)$$

In Eqs. (3.21) and (3.22) the following two results have been repeatedly used:

$$\int d\hat{n} Y_{\ell m}^*(\hat{n}) e^{-i\mu x} = \sqrt{4\pi} (-i)^\ell \sqrt{2\ell + 1} j_\ell(x), \quad (3.23)$$

$$\partial_\mu^2 [(1 - \mu^2)^2 e^{-i\mu x}] = \partial_\mu^2 [(1 + \partial_x^2)^2 e^{-i\mu x}] = -(1 + \partial_x^2) x^2 e^{-i\mu x}. \quad (3.24)$$

Furthermore, in Eq. (3.22), the equation of the spherical Bessel functions [68, 69] has been repeatedly used. Notice that, in Eq. (3.22) the integral over τ of the visibility function can be simplified by using, for $S_P(k, \mu, \tau)$, the expression of Eq. (3.19) and by performing exactly the same integral leading to Eq. (3.20).

In the present discussion we are interested in the scaling properties of the correlation functions over relatively small scales where simplifying expressions for the Bessel functions can be used. In this limit, the reionization effects can be parametrized as follows. In Eqs. (2.75) and (2.76) the integral over τ can be separated in two distinct contributions. For sake of concreteness consider the polarization integral which gives

$$\Delta_P(k, \mu, \tau_0) = \int_0^{\tau_{\text{re}}} d\tau \mathcal{K}(\tau) e^{-i\mu x} \tilde{S}_P(k, \mu, \tau) + \int_{\tau_{\text{re}}}^{\tau_0} d\tau \mathcal{K}(\tau) e^{-i\mu x} \tilde{S}_P(k, \mu, \tau). \quad (3.25)$$

The first term at the right hand side Eq. (3.25) is the most relevant for $\ell \gg 20$ and it is given by $e^{-\epsilon_{\text{re}}}\overline{\Delta}_{\text{P}}(k, \mu, \tau_0)$ where $\overline{\Delta}_{\text{P}}(k, \mu, \tau_0)$ is the value of the polarization in the absence of reionization. For small ℓ the second term in Eq. (3.25) is the most relevant [67] and it leads to supplementary peaks in the angular power spectra (i.e. the so-called reionization peaks). Within the approximations of this section, the integrand of the second term in Eq. (3.25) is simply proportional to the quadrupole of the intensity which can be evaluated, for $k < k_{\text{D}}$, as [67]

$$\Delta_{\text{I}2}(k, \mu, \tau_{\text{re}}) = \{\mathcal{L}(k, \tau_*) + \sqrt{c_{\text{sb}}}\mathcal{M}(k, \tau_*) \cos[kr_{\text{s}}(\tau_*)]\}j_2(x_{\text{re}}) \quad (3.26)$$

where $j_2(x_{\text{re}})$ is the spherical Bessel function for $\ell = 2$ and where $x_{\text{re}} = [k(\tau_{\text{re}} - \tau_*)]$. The reionization peaks arise, roughly, at the first peak of $j_2(x_{\text{re}})$, i.e. for $x_{\text{re}} \simeq 2$.

4 The basic integrals

4.1 Generalities

The considerations of the previous section depend upon two sorts of scales i.e.

- damping scales, (e. g. $\ell_{\text{D}}, \ell_{\text{t}}, \epsilon_{\text{re}}\dots$) which control the falloff of the temperature and polarization angular power spectra;
- oscillatory scales (e.g. ℓ_{A}) which control the structure of the peak and depths in the TT, EE and TE correlations.

The thermal diffusivity multipole ℓ_{D} , already introduced in Eq. (3.3), can be estimated using the best fit to the WMAP 5yr data alone [1, 2, 3]; Eq. (3.3) leads to $\ell_{\text{D}} = 1422.08$. The finite thickness of the visibility function leads to an effective multipole which can be estimated as $\ell_{\text{t}} = \sqrt{3}/(k_0\sigma_*)$. Again using the estimated thickness in the visibility function the WMAP 5yr data allow to estimate $\ell_{\text{t}} = 1211.22$. The typical scales ℓ_{D} and ℓ_{t} can be combined in what is often called Silk damping scale, i.e.

$$\frac{1}{\ell_{\text{S}}^2} = \frac{1}{\ell_{\text{t}}^2} + \frac{1}{\ell_{\text{D}}^2}, \quad \ell_{\text{S}} = \sqrt{\frac{\ell_{\text{t}}^2 \ell_{\text{D}}^2}{\ell_{\text{t}}^2 + \ell_{\text{D}}^2}}. \quad (4.1)$$

In the case of the numerical values listed above $\ell_{\text{S}} = 922.09$. The oscillatory patterns in the angular power spectra are determined by the acoustic multipole, i.e.

$$\begin{aligned} \ell_{\text{A}} &= \frac{\pi D_{\text{A}}(z_*)}{r_{\text{s}}(z_*)} = \frac{2\pi d_{\text{A}}(z_*)}{H_0\sqrt{\Omega_{\text{M}0}}r_{\text{s}}(z_*)} \equiv \frac{\sqrt{3R_{\text{b}*}}\pi\sqrt{z_*+1}d_{\text{A}}(z_*)}{\ln\left[\frac{\sqrt{1+R_{\text{b}*}}+\sqrt{(1+r_{\text{R}*})R_{\text{b}*}}}{1+\sqrt{r_{\text{R}*}R_{\text{b}*}}}\right]}, \\ &\equiv \left(\frac{z_*}{10^3}\right)^{1/2} \frac{\sqrt{R_{\text{b}*}}d_{\text{A}}(z_*)}{\ln\left[\frac{\sqrt{1+R_{\text{b}*}}+\sqrt{(1+r_{\text{R}*})R_{\text{b}*}}}{1+\sqrt{r_{\text{R}*}R_{\text{b}*}}}\right]}. \end{aligned} \quad (4.2)$$

The first equality of Eq. (4.2) is just the definition of the acoustic multipole while the second equality uses a more explicit form of the (comoving) angular diameter distance. Note that, in Eq. (4.2), the (reduced) angular diameter distance $d_A(z_*)$ goes asymptotically to 0.89 for $z_* > 500$ and for the standard values of the cosmological parameters. In the explicit expressions of some integrand it will prove useful to have an explicit expression also for $\gamma_A = \pi/\ell_A$: indeed, in various oscillating factors, the combination $\gamma_A \ell$ arises naturally. Thus Eq. (4.2) also implies

$$\gamma_A = \frac{\pi}{\ell_A} = \frac{1}{d_A(z_*)\sqrt{3R_{b*}(z_* + 1)}} \ln \left[\frac{\sqrt{1 + R_{b*}} + \sqrt{(1 + r_{R*})R_{b*}}}{1 + \sqrt{r_{R*}R_{b*}}} \right]. \quad (4.3)$$

According to Eq. (4.2), $\ell_A = 301.57$ while the WMAP 5yr data imply that the acoustic scale at decoupling is given by $\ell_A = 302.08_{-0.84}^{0.83}$. The acoustic multipole can be compared with the equality multipole, i.e.

$$\ell_{\text{eq}} = \sqrt{2\Omega_{\text{M}0}H_0} \sqrt{z_{\text{eq}} + 1} D_A(z_{\text{eq}}) = 2\sqrt{2} \sqrt{z_{\text{eq}}} \sqrt{\omega_{\text{M}}} = 2\sqrt{2} \sqrt{\frac{z_*}{r_{R*}}} d_A(z_*), \quad (4.4)$$

where we recalled that $\mathcal{H}_{\text{eq}} = a_{\text{eq}} H_{\text{eq}} = \sqrt{2\Omega_{\text{M}0}(a_0/a_{\text{eq}})^{1/2}}$. Combining the last equality of Eq. (4.4) with Eq. (3.5) we get $\ell_{\text{eq}} = 439.057 \sqrt{\omega_{\text{M}}} d_A(z_*)$ which also implies, in the case of the WMAP 5yr parameters, $\ell_{\text{eq}} \simeq 136.95$. In terms of ℓ_A the position of the first three Doppler peaks can be obtained approximately obtained from [15] $\ell_m = \ell_A(m - \varphi_m)$ where

$$\ell_1 = \ell_A(1 - \varphi_1), \quad \varphi_1 = 0.267 \left(\frac{r_{R*}}{0.3} \right)^{0.1}, \quad (4.5)$$

$$\ell_2 = \ell_A(2 - \varphi_2), \quad \varphi_2 = 0.24 \left(\frac{r_{R*}}{0.3} \right)^{0.1}, \quad (4.6)$$

$$\ell_3 = \ell_A(3 - \varphi_3), \quad \varphi_3 = 0.35 \left(\frac{r_{R*}}{0.3} \right)^{0.1}. \quad (4.7)$$

The values of ℓ_1 , ℓ_2 and ℓ_3 are deduced in the case $n_s = 1$. When $n_s \neq 1$ the positions are shifted as $\ell_m \rightarrow \ell_m + \Delta\ell_m$

$$\Delta\ell_1 = 0.13 |n_s - 1| \ell_1, \quad \Delta\ell_2 = 0.33 |n_s - 1| \ell_2, \quad \Delta\ell_3 = 0.61 |n_s - 1| \ell_3. \quad (4.8)$$

In the vanilla Λ CDM and for the WMAP 5yr best fit we have that

$$\ell_1 = 219, \quad \ell_2 = 535, \quad \ell_3 = 814. \quad (4.9)$$

which is approximately what could be obtained from Eqs. (4.7)–(4.8)

4.2 The angular power spectra

Using Eqs. (3.21) and (3.22) into Eqs. (2.60), (2.61) and (2.62) a more explicit expression of the angular power spectra can be obtained:

$$C_\ell^{(\text{TT})} = 4\pi \int \frac{dk}{k} \frac{k^3}{2\pi^2} |\Delta_\ell^{(\text{TT})}(k, \tau_0)|^2, \quad (4.10)$$

$$C_\ell^{(\text{EE})} = 4\pi \int \frac{dk}{k} \frac{k^3}{2\pi^2} |\Delta_\ell^{(\text{EE})}(k, \tau_0)|^2, \quad (4.11)$$

$$C_\ell^{(\text{TE})} = 4\pi \int \frac{dk}{k} \frac{k^3}{2\pi^2} |\Delta_\ell^{(\text{TE})}(k, \tau_0)|^2, \quad (4.12)$$

where the following quantities have been introduced:

$$|\Delta_\ell^{(\text{TT})}(k, \tau_0)|^2 = \left\{ |\Delta_{\text{I0}} + \psi|^2 + 9|\Delta_{\text{I1}}|^2 \left[1 - \frac{\ell(\ell+1)}{x^2} \right] \right\} j_\ell^2(x) e^{-2\frac{k^2}{k_t^2}}, \quad (4.13)$$

$$|\Delta_\ell^{(\text{EE})}(k, \tau_0)|^2 = 0.265 (k\sigma_*)^2 |\Delta_{\text{I1}}|^2 \ell(\ell-1)(\ell+1)(\ell+2) \frac{j_\ell^2(x)}{x^4}, \quad (4.14)$$

$$|\Delta_\ell^{(\text{TE})}(k, \tau_0)|^2 = 0.515 \sqrt{\ell(\ell-1)(\ell+1)(\ell+2)} (k\sigma_*) \Delta_{\text{I1}} (\Delta_{\text{I0}} + \psi) \frac{j_\ell^2(x)}{x^2} e^{-\frac{k^2}{k_t^2}}. \quad (4.15)$$

It is practical to adopt the following general parametrization for the three relevant power spectra of the problem

$$\mathcal{P}_\mathcal{R}(k) = \mathcal{A}_\mathcal{R} \left(\frac{k}{k_p} \right)^{n_s-1}, \quad \mathcal{P}_\Omega(k) = \mathcal{E}_\text{B} \left(\frac{k}{k_L} \right)^{2(n_B-1)}, \quad \mathcal{P}_\sigma(k) = r_B \mathcal{P}_\Omega(k), \quad (4.16)$$

where $\mathcal{A}_\mathcal{R}$ denotes the amplitude of the curvature perturbations at the pivot scale k_p ; \mathcal{E}_B denotes the amplitude of the power spectrum of Ω_B (see also [46, 48, 60]); r_B denotes the ratio⁸ between the power spectrum of σ_B and the power spectrum of Ω_B at the same magnetic pivot scale k_L . To leading order \mathcal{E}_B and r_B are independent upon the wave-number. There are however corrections which imply that \mathcal{E}_B and r_B do depend upon the wave-number. If $\mathcal{E}(k)$ and $r_B(k)$ the form of the integrals listed below as well as the related discussion slightly changes but the explicit results are more cumbersome and will not be reported here.

Using Eqs. (3.8) and (3.9) into Eqs. (4.13), (4.14) and (4.15) the explicit form of the temperature and polarization observables can be derived. Since some of the subsequent expressions are rather lengthy, the following rescaled amplitudes will be defined:

$$\begin{aligned} \mathcal{Q}_{\mathcal{R}\mathcal{R}} &= \mathcal{A}_\mathcal{R} \left(\frac{k_0}{k_p} \right)^{n_s-1} e^{-2\epsilon_{\text{re}}}, & \mathcal{Q}_{\text{BB}} &= \mathcal{E}_\text{B} \left(\frac{k_0}{k_L} \right)^{2(n_B-1)} e^{-2\epsilon_{\text{re}}}, \\ \mathcal{Q}_{\mathcal{R}\text{B}} &= \sqrt{\mathcal{A}_\mathcal{R}} \sqrt{\mathcal{E}_\text{B}} \left(\frac{k_0}{k_p} \right)^{\frac{n_s-1}{2}} \left(\frac{k_0}{k_L} \right)^{(n_B-1)} e^{-2\epsilon_{\text{re}}}, \end{aligned} \quad (4.17)$$

where $k_p = 0.002 \text{ Mpc}^{-1}$ is the pivot scale of curvature perturbations and, as already mentioned in section 2, $k_L = 1 \text{ Mpc}^{-1}$ is the magnetic pivot scale.

4.3 Temperature autocorrelations

The temperature autocorrelations are hereby written in terms of four basic integrals, i.e.

$$G_\ell^{(\text{TT})} = \mathcal{I}_{(1)}^{(\text{TT})}(\ell, \ell_t) + \mathcal{I}_{(2)}^{(\text{TT})}(\ell, \ell_S) + \mathcal{I}_{(3)}^{(\text{TT})}(\ell, \ell_S) + \mathcal{I}_{(4)}^{(\text{TT})}(\ell, \ell_t, \ell_S). \quad (4.18)$$

⁸It is often practical to assign ratios of power spectra at the same pivot scale; this is what happens also when assigning tensor power spectra in standard CMB studies.

Each of the terms appearing in Eq. (4.18) contains three contributions proportional, respectively, to $\mathcal{Q}_{\mathcal{R}\mathcal{R}}$, $\mathcal{Q}_{\mathcal{B}\mathcal{B}}$ and to $\mathcal{Q}_{\mathcal{R}\mathcal{B}}$ whose explicit form can be written as:

$$\mathcal{I}_{(1)}^{(\text{TT})}(\ell, \ell_t) = \mathcal{V}_{\mathcal{R}\mathcal{R}}^{(1)}(\ell, \ell_t) + \mathcal{V}_{\mathcal{B}\mathcal{B}}^{(1)}(\ell, \ell_t) + 2 \cos \beta \mathcal{V}_{\mathcal{R}\mathcal{B}}^{(1)}(\ell, \ell_t), \quad (4.19)$$

$$\mathcal{I}_{(2)}^{(\text{TT})}(\ell, \ell_s) = \mathcal{V}_{\mathcal{R}\mathcal{R}}^{(2)}(\ell, \ell_t) + \mathcal{V}_{\mathcal{B}\mathcal{B}}^{(2)}(\ell, \ell_t) + 2 \cos \beta \mathcal{V}_{\mathcal{R}\mathcal{B}}^{(2)}(\ell, \ell_t), \quad (4.20)$$

$$\mathcal{I}_{(3)}^{(\text{TT})}(\ell, \ell_s) = \mathcal{V}_{\mathcal{R}\mathcal{R}}^{(3)}(\ell, \ell_t) + \mathcal{V}_{\mathcal{B}\mathcal{B}}^{(3)}(\ell, \ell_t) + 2 \cos \beta \mathcal{V}_{\mathcal{R}\mathcal{B}}^{(3)}(\ell, \ell_t), \quad (4.21)$$

$$\mathcal{I}_{(4)}^{(\text{TT})}(\ell, \ell_s, \ell_t) = \mathcal{V}_{\mathcal{R}\mathcal{R}}^{(4)}(\ell, \ell_s, \ell_t) + \mathcal{V}_{\mathcal{B}\mathcal{B}}^{(4)}(\ell, \ell_s, \ell_t) + \cos \beta (\mathcal{V}_{\mathcal{R}\mathcal{B}}^{(4)} + \mathcal{V}_{\mathcal{B}\mathcal{R}}^{(4)})(\ell, \ell_s, \ell_t), \quad (4.22)$$

where $\cos \beta$ parametrizes the correlation between the purely adiabatic and the purely magnetized components⁹. The terms appearing in Eqs. (4.19) are expressible as

$$\mathcal{V}_{\mathcal{R}\mathcal{R}}^{(1)}(\ell, \ell_t) = \mathcal{Q}_{\mathcal{R}\mathcal{R}} \ell^{n_s-1} I_{\mathcal{R}\mathcal{R}}^{(1)}(\ell, \ell_t, n_s), \quad (4.23)$$

$$\mathcal{V}_{\mathcal{B}\mathcal{B}}^{(1)}(\ell, \ell_t) = \mathcal{Q}_{\mathcal{B}\mathcal{B}} \ell^{2(n_B-1)} I_{\mathcal{B}\mathcal{B}}^{(1)}(\ell, \ell_t, 2n_B - 1), \quad (4.24)$$

$$\mathcal{V}_{\mathcal{R}\mathcal{B}}^{(1)}(\ell, \ell_t) = \mathcal{Q}_{\mathcal{R}\mathcal{B}} \ell^{\frac{n_s+2n_B-3}{2}} I_{\mathcal{R}\mathcal{B}}^{(1)}\left(\ell, \ell_t, \frac{n_s + 2n_B - 1}{2}\right). \quad (4.25)$$

The basic integral appearing in Eqs. (4.23)–(4.25) is given by¹⁰:

$$I_{XY}^{(1)}(\ell, \ell_t, n) = \int_1^\infty \frac{w^{n-3}}{\sqrt{w^2-1}} L_X(w, \ell) L_Y(w, \ell) e^{-2(\frac{\ell^2}{\ell_t^2})w^2} dw. \quad (4.26)$$

In Eqs. (4.26) the functions $L_X(w, \ell)$ and $L_Y(w, \ell)$ account for the contribution of large-scale magnetic fields to the tight coupling solutions and also depend upon the resolution of the calculation, i.e. upon ℓ_{max} (which denotes the maximal multipole at which the calculation is trustable). The four functions which enter Eq. (4.26) as well as the other seven integrals which will be discussed below are:

$$L_{\mathcal{R}}(w, \ell) = \alpha_{\mathcal{R}} - \beta_{\mathcal{R}} \ln(w q \ell), \quad L_{\mathcal{B}}(w, \ell) = \alpha_{\mathcal{B}} - \beta_{\mathcal{B}} \ln(w q \ell), \quad (4.27)$$

$$M_{\mathcal{R}}(w, \ell) = \bar{\alpha}_{\mathcal{R}} + \bar{\beta}_{\mathcal{R}} \ln(w q \ell), \quad M_{\mathcal{B}}(w, \ell) = \bar{\alpha}_{\mathcal{B}} + \bar{\beta}_{\mathcal{B}} \ln(w q \ell), \quad (4.28)$$

where

$$\alpha_{\mathcal{R}} = \frac{R_b}{6} \ln\left(\frac{7}{100}\right), \quad \beta_{\mathcal{R}} = \frac{R_b}{6}, \quad (4.29)$$

$$\bar{\alpha}_{\mathcal{R}} = -\frac{6}{25} \ln(96), \quad \bar{\beta}_{\mathcal{R}} = -\frac{6}{25}, \quad (4.30)$$

$$\alpha_{\mathcal{B}} = r_B - \frac{3R_\gamma r_B + 5}{20}, \quad \beta_{\mathcal{B}} = 0, \quad (4.31)$$

$$\bar{\alpha}_{\mathcal{B}} = [3(R_b + 1)]^{1/4} \left[\frac{R_\gamma + 5}{20} - r_B \right], \quad \bar{\beta}_{\mathcal{B}} = 0, \quad (4.32)$$

⁹This correlation arises, in explicit models, because magnetic fields are produced during some stages of inflationary expansion [23] (see also [24, 25, 26, 27]). In a model-independent perspective the correlation between different components should also be considered in full analogy with what happens for entropic initial conditions [50, 51, 52, 53, 54].

¹⁰It is relevant to point out that the arguments of the integrals contain the multipole, the diffusion scales and the relevant spectral index. These are the basic quantities which define the eight basic integrals which will now be listed.

where R_b is the baryon to photon ratio at the recombination and q_ℓ is given by:

$$q_\ell = \left(\frac{\ell}{200 d_A(z_*)} \right) \sqrt{\frac{r_{R*}}{z_* + 1}}. \quad (4.33)$$

Concerning the notations of Eqs. (4.29)–(4.32) we remind, as defined after Eq. (4.16) that $r_B = \mathcal{P}_\Omega/\mathcal{P}_\sigma$: r_B is, therefore, the ratio between the power spectrum associated with Ω_B and the power spectrum associated with σ_B .

Since the aim of the present analysis is to have analytic estimates of the modifications induced by large-scale magnetic fields especially at small angular scales (i.e. in the limit $\ell \gg 1$). In the latter limit the spherical Bessel functions $j_\ell(x)$ can be approximated in their large-order limit and the acoustic multipole fixes the oscillatory structure of the angular power spectra:

$$\ell(\ell + 1)j_\ell^2(x) \simeq \ell(\ell + 1) \frac{\cos^2[\beta(x, \ell)]}{x\sqrt{x^2 - \ell^2}} \simeq \frac{1}{2w\sqrt{w^2 - 1}}, \quad x = w\ell, \quad (4.34)$$

where $\beta(x, \ell) = \sqrt{x^2 - \ell^2} - \ell \arccos(\ell/x) - \frac{\pi}{4}$ [68, 69]. Recall that, often, changes of variables are required to evaluate the integrals. In particular, a practical choice is:

$$w \rightarrow y^2 + 1, \quad dw \rightarrow 2ydy, \quad \frac{dw}{\sqrt{w^2 - 1}} \rightarrow \frac{2dy}{\sqrt{y^2 + 2}}. \quad (4.35)$$

The change of variable $w^2 = y^2 + 1$ is also possible in some cases and it leads to a simpler structure of the integrands, in some cases. In spite of the change of variables, the numerical values of the various integrals do not change. At the same time, since the integrals will be evaluated numerically, the time of evaluation can also change as a function of the algebraic form of the various integrands.

The contribution labeled by $\mathcal{I}_{(2)}^{(\Gamma\Gamma)}(\ell, \ell_S)$ in Eqs. (4.18) and (4.20) leads to the following explicit results

$$\mathcal{V}_{\mathcal{RR}}^{(2)}(\ell, \ell_S) = \mathcal{Q}_{\mathcal{RR}} \ell^{n_s - 1} I_{\mathcal{RR}}^{(2)}(\ell, \ell_S, n_s), \quad (4.36)$$

$$\mathcal{V}_{\mathcal{BB}}^{(2)}(\ell, \ell_S) = \mathcal{Q}_{\mathcal{BB}} \ell^{2(n_B - 1)} I_{\mathcal{BB}}^{(2)}(\ell, \ell_S, 2n_B - 1), \quad (4.37)$$

$$\mathcal{V}_{\mathcal{RB}}^{(2)}(\ell, \ell_t) = \mathcal{Q}_{\mathcal{RB}} \ell^{\frac{n_s + 2n_B - 3}{2}} I_{\mathcal{RB}}^{(2)}\left(\ell, \ell_S, \frac{n_s + 2n_B - 1}{2}\right), \quad (4.38)$$

where the second basic integral appearing in Eqs. (4.36)–(4.38) can be written as:

$$I_{XY}^{(2)}(\ell, \ell_t, n) = \frac{1}{2} \int_1^\infty \mathcal{W}_+(w, c_{sb}) w^{n-5} M_X(w, \ell) M_Y(w, \ell) e^{-2(\frac{\ell^2}{\ell_S^2})w^2} dw. \quad (4.39)$$

For practical convenience, the two functions $\mathcal{W}_\pm(w, c_{sb})$ are introduced, respectively, in Eq. (4.39) and in Eq. (4.44):

$$\mathcal{W}_\pm(w, c_{sb}) = \frac{c_{sb}(1 \pm 9c_{sb}^2)w^2 \mp 9c_{sb}^3}{\sqrt{w^2 - 1}}, \quad (4.40)$$

where c_{sb} is the photon-baryon sound speed already introduced, for instance, in Eq. (1.4). The third contribution appearing in Eq. (4.18), i.e. $\mathcal{I}_3^{(\text{TT})}(\ell, \ell_S)$ is determined by the terms appearing in Eq. (4.21) whose explicit expressions are:

$$\mathcal{V}_{\mathcal{RR}}^{(3)}(\ell, \ell_S) = \mathcal{Q}_{\mathcal{RR}} \ell^{n_s-1} I_{\mathcal{RR}}^{(3)}(\ell, \ell_S, n_s), \quad (4.41)$$

$$\mathcal{V}_{\text{BB}}^{(3)}(\ell, \ell_S) = \mathcal{Q}_{\text{BB}} \ell^{2(n_B-1)} I_{\text{BB}}^{(3)}(\ell, \ell_S, 2n_B - 1), \quad (4.42)$$

$$\mathcal{V}_{\mathcal{RB}}^{(3)}(\ell, \ell_t) = \mathcal{Q}_{\mathcal{RB}} \ell^{\frac{n_s+2n_B-3}{2}} I_{\mathcal{RB}}^{(3)}\left(\ell, \ell_S, \frac{n_s + 2n_B - 1}{2}\right). \quad (4.43)$$

Recalling Eq. (4.40) the basic integral appearing in Eqs. (4.41)–(4.43) is given by:

$$I_{XY}^{(3)}(\ell, \ell_S, n) = \frac{1}{2} \int_1^\infty \mathcal{W}_-(w, c_{\text{sb}}) w^{n-5} \cos(2\gamma_A \ell w) M_X(w, \ell) M_Y(w, \ell) e^{-2\left(\frac{\ell^2}{\ell_S^2}\right)w^2} dw, \quad (4.44)$$

where γ_A has been introduced in Eq. (4.3) and $\mathcal{W}_-(w, c_{\text{sb}})$ is defined in Eq. (4.40). Finally, the fourth basic term of Eqs. (4.18) and (4.22) is completely specified by the four expressions:

$$\mathcal{V}_{\mathcal{RR}}^{(4)}(\ell, \ell_S) = \mathcal{Q}_{\mathcal{RR}} \ell^{n_s-1} I_{\mathcal{RR}}^{(4)}(\ell, \ell_S, \ell_t, n_s), \quad (4.45)$$

$$\mathcal{V}_{\text{BB}}^{(4)}(\ell, \ell_S) = \mathcal{Q}_{\text{BB}} \ell^{2(n_B-1)} I_{\text{BB}}^{(4)}(\ell, \ell_S, \ell_t, 2n_B - 1), \quad (4.46)$$

$$\mathcal{V}_{\mathcal{RB}}^{(4)}(\ell, \ell_t) = \mathcal{Q}_{\mathcal{RB}} \ell^{\frac{n_s+2n_B-3}{2}} I_{\mathcal{RB}}^{(4)}\left(\ell, \ell_S, \frac{n_s + 2n_B - 1}{2}\right). \quad (4.47)$$

The basic integral appearing in Eqs. (4.41)–(4.43) is given by:

$$I_{XY}^{(4)}(\ell, \ell_S, \ell_t, n) = 2 \int_1^\infty \frac{\sqrt{c_{\text{sb}}} w^{n-3}}{\sqrt{w^2 - 1}} \cos(\gamma_A \ell w) L_X(w, \ell) M_Y(w, \ell) e^{-\left[\left(\frac{\ell^2}{\ell_S^2}\right) + \left(\frac{\ell^2}{\ell_t^2}\right)\right]w^2} dw. \quad (4.48)$$

Equations (4.26), (4.39), (4.44) and (4.48) define the primary form of the integrals determining the temperature autocorrelations. In what follows the EE and TE correlations will be more specifically studied.

4.4 E-mode autocorrelations

Within the same logical scheme already employed in the case of the TT correlations, the EE angular power spectra of Eq. (4.11) can be written in terms of two (further) basic integrals, i.e.

$$G_\ell^{(\text{EE})} = \mathcal{I}_{(5)}^{(\text{EE})}(\ell, \ell_D) - \mathcal{I}_{(6)}^{(\text{EE})}(\ell, \ell_D). \quad (4.49)$$

Both the EE and the TE angular power spectra are suppressed with respect to the TT correlations. It is therefore useful to define the quantity

$$\mathcal{N}^{(\text{EE})}(\ell, \sigma_*) = 0.132 (k_0 \sigma_*)^2 (\ell + 1)^2 (\ell - 1) (\ell + 2) \ell^{-4}, \quad (4.50)$$

which is independent of ℓ in the range of multipoles where the calculation can be trusted (i.e., in practice, $\ell > 20$). The explicit form of the integrals appearing in Eq. (4.49) can be

written, in full analogy with Eqs. (4.19)–(4.22), as

$$\mathcal{I}_{(5)}^{(\text{EE})}(\ell, \ell_{\text{D}}) = \mathcal{V}_{\mathcal{RR}}^{(5)}(\ell, \ell_{\text{D}}) + \mathcal{V}_{\text{BB}}^{(5)}(\ell, \ell_{\text{D}}) + 2 \cos \beta \mathcal{V}_{\mathcal{RB}}^{(5)}(\ell, \ell_{\text{D}}), \quad (4.51)$$

$$\mathcal{I}_{(6)}^{(\text{EE})}(\ell, \ell_{\text{D}}) = \mathcal{V}_{\mathcal{RR}}^{(6)}(\ell, \ell_{\text{D}}) + \mathcal{V}_{\text{BB}}^{(6)}(\ell, \ell_{\text{D}}) + 2 \cos \beta \mathcal{V}_{\mathcal{RB}}^{(6)}(\ell, \ell_{\text{D}}). \quad (4.52)$$

where

$$\mathcal{V}_{\mathcal{RR}}^{(5)}(\ell, \ell_{\text{D}}) = \mathcal{Q}_{\mathcal{RR}} \mathcal{N}^{(\text{EE})}(\ell, \sigma_*) \ell^{n_{\text{s}}+1} c_{\text{sb}}^3 I_{\mathcal{RR}}^{(5)}(\ell, \ell_{\text{D}}, n_{\text{s}}), \quad (4.53)$$

$$\mathcal{V}_{\text{BB}}^{(5)}(\ell, \ell_{\text{D}}) = \mathcal{Q}_{\text{BB}} \mathcal{N}^{(\text{EE})}(\ell, \sigma_*) \ell^{2n_{\text{B}}} c_{\text{sb}}^3 I_{\text{BR}}^{(5)}(\ell, \ell_{\text{D}}, 2n_{\text{B}} - 1) \quad (4.54)$$

$$\mathcal{V}_{\mathcal{RB}}^{(5)}(\ell, \ell_{\text{D}}) = \mathcal{Q}_{\mathcal{RB}} \mathcal{N}^{(\text{EE})}(\ell, \sigma_*) \ell^{\frac{n_{\text{s}}+2n_{\text{B}}+1}{2}} c_{\text{sb}}^3 I_{\mathcal{RB}}^{(5)}\left(\ell, \ell_{\text{D}}, \frac{n_{\text{s}} + 2n_{\text{B}} - 1}{2}\right), \quad (4.55)$$

where

$$I_{XY}^{(5)}(\ell, \ell_{\text{D}}, n) = \int_1^\infty \frac{w^{n-5}}{\sqrt{w^2 - 1}} M_X(w, \ell) M_Y(w, \ell) e^{-2(\frac{\ell^2}{\ell_{\text{D}}^2})w^2} dw. \quad (4.56)$$

The three terms defining $\mathcal{I}_{(6)}^{(\text{EE})}(\ell, \ell_{\text{D}})$ are:

$$\mathcal{V}_{\mathcal{RR}}^{(6)}(\ell, \ell_{\text{D}}) = \mathcal{Q}_{\mathcal{RR}} \mathcal{N}^{(\text{EE})}(\ell, \sigma_*) \ell^{n_{\text{s}}-3} c_{\text{sb}}^3 I_{\mathcal{RR}}^{(6)}(\ell, \ell_{\text{D}}, n_{\text{s}}), \quad (4.57)$$

$$\mathcal{V}_{\text{BB}}^{(6)}(\ell, \ell_{\text{D}}) = \mathcal{Q}_{\text{BB}} \mathcal{N}^{(\text{EE})}(\ell, \sigma_*) \ell^{2n_{\text{B}}-4} c_{\text{sb}}^3 I_{\text{BR}}^{(6)}(\ell, \ell_{\text{D}}, 2n_{\text{B}} - 1), \quad (4.58)$$

$$\mathcal{V}_{\mathcal{RB}}^{(6)}(\ell, \ell_{\text{D}}) = \mathcal{Q}_{\mathcal{RB}} \mathcal{N}^{(\text{EE})}(\ell, \sigma_*) \ell^{\frac{n_{\text{s}}+2n_{\text{B}}-7}{2}} c_{\text{sb}}^3 I_{\mathcal{RB}}^{(6)}\left(\ell, \ell_{\text{D}}, \frac{n_{\text{s}} + 2n_{\text{B}} - 1}{2}\right). \quad (4.59)$$

The sixth basic integral appearing in Eqs. (4.57)–(4.59) is

$$I_{XY}^{(6)}(\ell, \ell_{\text{D}}, n) = \int_1^\infty \frac{\cos(2\gamma_{\text{A}} \ell w) w^{n-5}}{\sqrt{w^2 - 1}} dw M_X(w, \ell) M_Y(w, \ell) e^{-2(\frac{\ell^2}{\ell_{\text{D}}^2})w^2}. \quad (4.60)$$

Equations (4.56) and (4.60) represent the primary form of the two basic integrals determining the polarization autocorrelations. From the purely algebraic point of view the EE angular power spectra have a single periodicity is insofar as Eq. (4.56) has an integrand which is not oscillating while the integrand of Eq. (4.60) depends on a single oscillating term. Conversely, the TT angular power spectra are given by the weighted superposition of the integrals appearing in Eqs. (4.26), (4.39), (4.44) and (4.48) whose corresponding integrals do not depend upon the same oscillating term. The single periodicity of the EE angular power spectra will, have, in the present context, interesting consequences.

4.5 Temperature-polarization cross-correlations

The last angular power spectrum considered here is the one arising from the cross-correlations between temperature and polarization, i.e. the TE power spectrum leading to the following integrals

$$G_\ell^{(\text{TE})} = \mathcal{I}_{(7)}^{(\text{TE})}(\ell, \ell_{\text{S}}) + \mathcal{I}_{(8)}^{(\text{TE})}(\ell, \ell_{\text{S}}, \ell_{\text{D}}). \quad (4.61)$$

In full analogy with what has been done in the case of the EE correlations (see Eq. (4.50)) it is practical to define

$$\mathcal{N}^{(\text{TE})}(\ell, \sigma_*) = 0.515 k_0 \sigma_* (\ell + 1) \sqrt{(\ell + 1)(\ell - 1)(\ell + 2)} \ell^{-5/2}. \quad (4.62)$$

Consequently, the explicit form of the integrals appearing in Eq. (4.61) is

$$\mathcal{I}_7^{(\text{TE})}(\ell, \ell_S) = \mathcal{V}_{\mathcal{RR}}^{(7)}(\ell, \ell_S) + \mathcal{V}_{\text{BB}}^{(7)}(\ell, \ell_S) + \cos \beta [\mathcal{V}_{\mathcal{RB}}^{(7)}(\ell, \ell_S) + \mathcal{V}_{\text{BR}}^{(7)}(\ell, \ell_S)], \quad (4.63)$$

$$\mathcal{I}_8^{(\text{TE})}(\ell, \ell_S, \ell_D) = \mathcal{V}_{\mathcal{RR}}^{(8)}(\ell, \ell_S, \ell_D) + \mathcal{V}_{\text{BB}}^{(8)}(\ell, \ell_S, \ell_D) + 2 \cos \beta \mathcal{V}_{\mathcal{RB}}^{(8)}(\ell, \ell_S, \ell_D). \quad (4.64)$$

where

$$\mathcal{V}_{\mathcal{RR}}^{(7)}(\ell, \ell_S) = \mathcal{Q}_{\mathcal{RR}} \mathcal{N}^{(\text{TE})}(\ell, \sigma_*) \ell^{n_s} c_{\text{sb}}^{3/2} I_{\mathcal{RR}}^{(7)}(\ell, \ell_S, n_s), \quad (4.65)$$

$$\mathcal{V}_{\text{BB}}^{(7)}(\ell, \ell_S) = \mathcal{Q}_{\text{BB}} \mathcal{N}^{(\text{TE})}(\ell, \sigma_*) \ell^{2n_B - 1} c_{\text{sb}}^{3/2} I_{\text{BB}}^{(7)}(\ell, \ell_S, 2n_B - 1) \quad (4.66)$$

$$\mathcal{V}_{\mathcal{RB}}^{(7)}(\ell, \ell_S) = \mathcal{Q}_{\mathcal{RB}} \mathcal{N}^{(\text{TE})}(\ell, \sigma_*) c_{\text{sb}}^{3/2} \ell^{\frac{n_s + 2n_B - 1}{2}} I_{\mathcal{RB}}^{(7)}\left(\ell, \ell_S, \frac{n_s + 2n_B - 1}{2}\right). \quad (4.67)$$

The integral appearing in Eqs. (4.65)–(4.67)

$$I_{XY}^{(7)}(\ell, \ell_S, n) = \int_1^\infty \frac{\sin(\gamma_A \ell w) w^{n-4}}{\sqrt{w^2 - 1}} dw L_X(w, \ell) M_Y(w, \ell) e^{-\left(\frac{\ell^2}{\ell_S^2}\right) w^2}. \quad (4.68)$$

The last bunch of terms contributing to $\mathcal{I}_8^{(\text{TE})}(\ell, \ell_S, \ell_D)$ is given by

$$\mathcal{V}_{\mathcal{RR}}^{(8)}(\ell, \ell_S, \ell_D) = \mathcal{Q}_{\mathcal{RR}} \mathcal{N}^{(\text{TE})}(\ell, \sigma_*) \ell^{n_s} c_{\text{sb}}^2 I_{\mathcal{RR}}^{(8)}(\ell, \ell_S, \ell_D, n_s), \quad (4.69)$$

$$\mathcal{V}_{\text{BB}}^{(8)}(\ell, \ell_S) = \mathcal{Q}_{\text{BB}} \mathcal{N}^{(\text{TE})}(\ell, \sigma_*) \ell^{2n_B - 1} c_{\text{sb}}^2 I_{\text{BB}}^{(8)}(\ell, \ell_S, \ell_D, 2n_B - 1), \quad (4.70)$$

$$\mathcal{V}_{\mathcal{RB}}^{(8)}(\ell, \ell_S, \ell_D) = \mathcal{Q}_{\mathcal{RB}} \mathcal{N}^{(\text{TE})}(\ell, \sigma_*) \ell^{\frac{n_s + 2n_B - 7}{2}} c_{\text{sb}}^2 I_{\mathcal{RB}}^{(8)}\left(\ell, \ell_S, \ell_D, \frac{n_s + 2n_B - 1}{2}\right), \quad (4.71)$$

where

$$I_{XY}^{(8)}(\ell, \ell_S, \ell_D, n) = \frac{1}{2} \int_1^\infty \frac{\sin(2\gamma_A \ell w) w^{n-4}}{\sqrt{w^2 - 1}} dw M_X(w, \ell) M_Y(w, \ell) e^{-\left(\frac{\ell^2}{\ell_S^2} + \frac{\ell^2}{\ell_D^2}\right) w^2}. \quad (4.72)$$

The integrals of Eqs. (4.68) and (4.72) give the last pair of primary integrals. The results obtained in the present section allow for an explicit evaluation of the TT, EE and TE angular power spectra. The following section is devoted to the derivation of a number of scaling relations which are the magnetized analog of the standard scaling relations which constitute the basis of any sound strategy of parameter estimation.

5 Scaling properties and form factors

The 8 basic integrals derived in section 4 can be exploited to study the deviations induced by the ambient magnetic field on the CMB observables. In the present section the semi-analytic

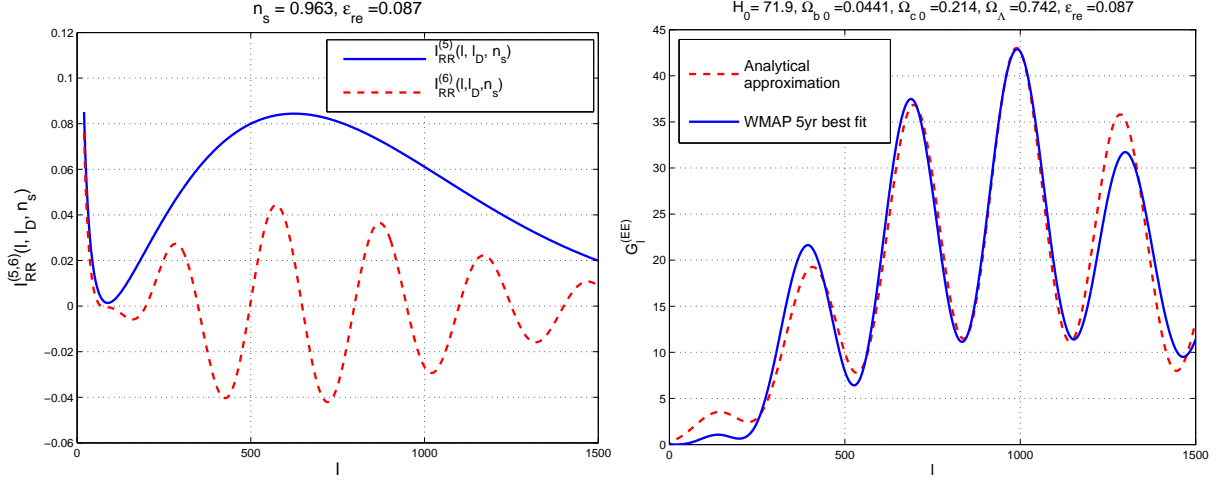


Figure 3: The semi-analytic results for the polarization autocorrelations are illustrated in the absence of magnetic fields. In the plot at the left, the explicit result for the integrals of Eq. (5.5) is reported. In the plot at the right the explicit result of Eqs. (5.6)–(5.7) is confronted to the WMAP 5yr best fit.

results will be confronted with the numerical estimates. The purpose will not be to touch upon all the possible themes of the analysis but rather to mention only some of the most notable aspects which emerged from an exhaustive study of these matters. The polarization autocorrelations are sensitive to 2 out of 8 basic integrals and, as previously discussed (see, e.g. discussion after Eq. (4.60)), they have the simpler periodicity. They also depend upon ℓ_D since the integral over the optical depth allows for an explicit integration of the source term (see Eqs. (3.15)–(3.19)). The present section is organized as follows: in subsection 5.1 the EE angular power spectra will be discussed and the semi-analytical results will be compared with the numerical evaluation. In subsection 5.2 the semi-analytical results for the TT and TE correlations will be illustrated. Finally, subsection 5.3 will be focussed on the scaling properties of the temperature and polarization autocorrelations.

5.1 EE angular power spectra

In the absence of any ambient magnetic field, Eqs. (4.49) and (4.51)–(4.52) lead to the complete expression of the EE correlation which can be written as

$$\begin{aligned}
 G_\ell^{(\text{EE})} &= \mathcal{I}_{(5)}^{(\text{EE})}(\ell, \ell_D) - \mathcal{I}_{(6)}^{(\text{EE})}(\ell, \ell_D), \\
 \mathcal{I}_{(5)}^{(\text{EE})}(\ell, \ell_D) &= \mathcal{V}_{\mathcal{RR}}^{(5)}(\ell, \ell_D), \quad \mathcal{I}_{(6)}^{(\text{EE})}(\ell, \ell_D) = \mathcal{V}_{\mathcal{RR}}^{(6)}(\ell, \ell_D).
 \end{aligned} \tag{5.1}$$

Bearing in mind the explicit form of the different contributions, Eq. (5.1) becomes

$$G_\ell^{(\text{EE})} = \overline{\mathcal{A}}^{(\text{EE})}(\ell - 1)(\ell + 1)^2(\ell + 2)\ell^{n_s - 3}[\mathcal{I}_{\mathcal{RR}}^{(5)}(\ell, \ell_D, n_s) - \mathcal{I}_{\mathcal{RR}}^{(6)}(\ell, \ell_D, n_s)], \tag{5.2}$$

$$\overline{\mathcal{A}}^{(\text{EE})} = (0.132) (k_0 \sigma_*)^2 \left(\frac{k_0}{k_p}\right)^{n_s-1} c_{\text{sb}}^3 e^{-2\epsilon_{\text{re}}} \mathcal{A}_{\mathcal{R}} T_{\gamma_0}^2 \quad (5.3)$$

where $\overline{\mathcal{A}}^{(\text{EE})}$ is the rescaled amplitude grouping all the factors which are independent on the multipole ℓ . If $n_s = 0.963$ and $\epsilon_{\text{re}} = 0.087$ (as in the 5yr best fit to the WMAP data alone), Eq. (5.3) implies that ¹¹ $\overline{\mathcal{A}}^{(\text{EE})} = 4.25 \times 10^{-4} (\mu\text{K})^2$. The factor $(k_0 \sigma_*)$ can be estimated within the WMAP data and it is given by 1.43×10^{-3} . The latter figure arises, as discussed after Eq. (2.35), by computing $\Delta\tau_*/\tau_0$ where $\Delta\tau_*$ is the thickness of the last scattering surface in conformal time. The integrals of Eq. (5.2) appeared already in Eqs. (4.56) and

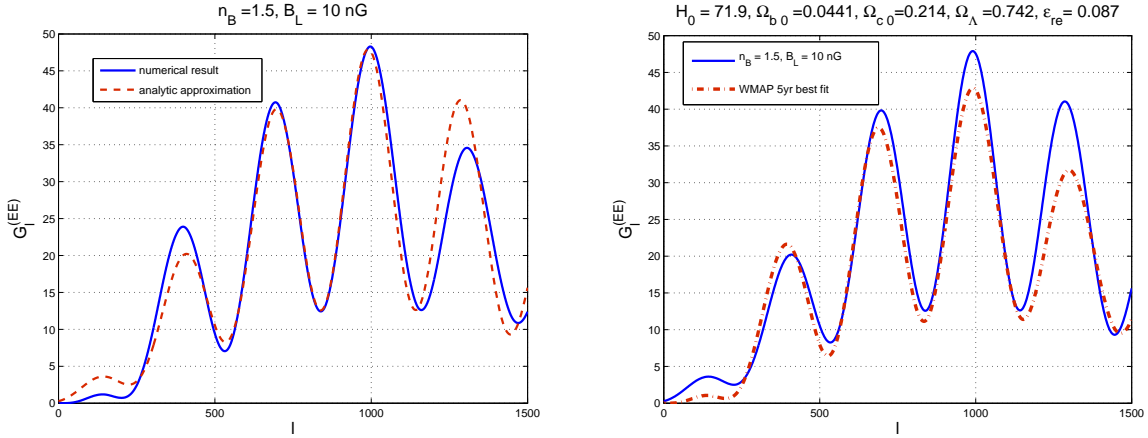


Figure 4: The semi-analytic results for the polarization autocorrelations are illustrated in the presence of magnetic fields. In the left plot the full line denotes the numerical result while the dashed line denotes the analytic approximation. In the right plot the magnetized result is compared with the WMAP best fit. In this and in the following plots $\beta = 0$.

(4.60) and their explicit expressions, for the case at hand, is:

$$\begin{aligned} I_{\mathcal{R}\mathcal{R}}^{(5)}(\ell, \ell_D, n_s) &= \int_1^\infty dw \frac{w^{n_s-5}}{\sqrt{w^2-1}} M_{\mathcal{R}}^2(w, \ell) e^{-2(\ell/\ell_D)^2 w^2}, \\ I_{\mathcal{R}\mathcal{R}}^{(6)}(\ell, \ell_D, n_s) &= \int_1^\infty dw \frac{w^{n_s-5}}{\sqrt{w^2-1}} \cos[2\gamma_A \ell w] M_{\mathcal{R}}^2(w, \ell) e^{-2(\ell/\ell_D)^2 w^2}. \end{aligned} \quad (5.4)$$

It is possible to change integration variable in Eqs. (5.4). By positing $w = y^2 + 1$ we do get¹²:

$$\mathcal{I}_{\mathcal{R}\mathcal{R}}^{(5)}(\ell, \ell_D, n_s) = 2 \int_0^\infty dy \frac{(y^2 + 1)^{n_s-5}}{\sqrt{y^2 + 2}} M_{\mathcal{R}}^2(y, \ell) e^{-2(\frac{\ell^2}{\ell_D^2})(y^2+1)^2},$$

¹¹It should be noticed that the expression for $\overline{\mathcal{A}}^{(\text{EE})}$ is dimension-full since the result has been multiplied, as customary, by $T_{\gamma_0}^2 = (2.725 \times 10^6)^2 (\mu\text{K})^2$ where T_{γ_0} is the inferred value of the CMB black-body spectrum in units of μK .

¹²The change of variable $w^2 = y^2 + 1$ is also possible and, in this particular case, will lead, of course, to the same results. In the case of other integrals, however, mathematically equivalent change of variables might lead to different evaluation times of the corresponding numerical integrals.

$$\mathcal{I}_{\mathcal{R}\mathcal{R}}^{(6)}(\ell, \ell_D, n_s) = 2 \int_0^\infty dy \frac{(y^2 + 1)^{n_s - 5}}{\sqrt{y^2 + 2}} \cos[2\gamma_A \ell (y^2 + 1)] M_{\mathcal{R}}^2(y, \ell) e^{-2(\frac{\ell^2}{\ell_D^2})(y^2 + 1)^2}. \quad (5.5)$$

The integrals of Eq. (5.5) converge rapidly and can be estimated, for instance, with numerical techniques; the final result can be expressed in a closed form for $\ell > \ell_1$ as

$$G_\ell^{(\text{EE})} = \overline{\mathcal{A}}^{(\text{EE})} (\ell + \ell_1)^{n_s + 1} \left\{ a_E - b_E \cos[2\gamma_A (\ell + \ell_1)] \right\} e^{-2(\ell/\ell_D)^2}, \quad (5.6)$$

$$\overline{\mathcal{A}}^{(\text{EE})} = 4.476 \times 10^{-4} (0.0354)^{n_s - 1} \left(\frac{\mathcal{A}_{\mathcal{R}}}{2.41 \times 10^{-9}} \right) e^{-2\epsilon_{\text{re}}} (\mu\text{K})^2, \quad (5.7)$$

$$a_E = 1.67, \quad b_E = 3.38, \quad \ell_1 = 65, \quad (5.8)$$

where ℓ_1 appears because the analytic derivations of the previous sections assume a large-order expression for the spherical Bessel functions. Concerning Eq. (5.7) few comments are in order:

- Eq. (5.7) assumes the simplified treatment of reionization which has been spelled out in Eqs. (3.25)–(3.26) and which is less accurate for low multipoles (i.e. in the region of the reionization peaks) than for large multipoles;
- a_E and b_E are, respectively, the form factors coming from the integral $\mathcal{I}_{\mathcal{R}\mathcal{R}}^{(5)}(\ell, \ell_D, n_s)$ and from $\mathcal{I}_{\mathcal{R}\mathcal{R}}^{(6)}(\ell, \ell_D, n_s)$;
- ℓ_D (i.e. the diffusion damping scale) is given by Eq. (3.3) and has been also discussed prior to Eq. (4.1) in connection with the estimate of Silk damping;
- the numerical value of $\mathcal{A}^{(\text{EE})}$ follows from the pivotal value of k_p (i.e. 0.002 Mpc^{-1}) and by computing k_0 from the (comoving) angular diameter distance of Eq. (3.4);

In terms of the values of the cosmological parameters obtainable from the WMAP 5yr best fit [1, 2, 3]

$$(\omega_M, \omega_c, \omega_b, \omega_\Lambda, h_0, n_s, \epsilon_{\text{re}}) \equiv (0.1326, 0.1099, 0.02273, 0.385, 0.719, 0.963, 0.087), \quad (5.9)$$

the values of the derived parameters of Eqs. (3.3)–(3.6) are¹³

$$[z_*, c_{\text{sb}}(z_*), D_A(z_*), \ell_A, \ell_D, \ell_t, \ell_S] = [1099.5, 0.451, 14110.8 \text{ Mpc}, 301.578, 1422, 1211, 922]. \quad (5.10)$$

The results for the polarization autocorrelations are illustrated in Fig. 3. In the plot at the left $\mathcal{I}_{\mathcal{R}\mathcal{R}}^{(5)}(\ell, \ell_D, n_s)$ and $\mathcal{I}_{\mathcal{R}\mathcal{R}}^{(6)}(\ell, \ell_D, n_s)$ are reported, respectively, with the full and with the dashed lines. In the plot at the right of Fig. 3 the analytic result for $G_\ell^{(\text{EE})}$ (dashed

¹³Different best-fit parameters, obtained by combining CMB data with other data sets (e.g. [79, 80]) lead to different values of the derived parameters which can be however computed always using the general formulae of the previous sections.

line) is compared with the WMAP 5yr best fit (full line) holding for exactly the same set of parameters (i.e. Eq. (5.9)). In Fig. 4 the analytic results for the magnetized polarization autocorrelations are compared with the numerical results. In both plots of Fig. 4 the numerical result is reported with the full line. The dashed line denotes the analytical approximation (plot at the left). The dot-dashed line denotes the WMAP 5yr best fit (for the same value of cosmological parameters). In both plots the correlation angle has been chosen as $\beta = 0$. In summary we can therefore say that Figs. 3 and 4 show that, in spite of the different approximations, the analytic result is in fair agreement with the numerical one. Finally, the numerical results illustrated in Figs. 4 and 5 follow from an improved version of the approach already mentioned in the introduction [48, 49] which is based on a modification of CMBFAST [81, 82] (which is, in turn, a modified version of Cosmics [83, 84]).

5.2 TT and TE angular power spectra

The TT and TE correlations share similar features from the point of view of the analytical results discussed here. The periodicities of the TT and TE angular power spectra arise as the weighted interference of the periodicities of the monopole and of the dipole of the radiation field. The TT correlations, have been partially discussed with a similar semi-analytic method in [48] (first paper) and corroborated by subsequent numerical estimates (second paper of [48]). The improved analytical understanding developed in the present paper allows for a better assessment of the accuracy of the results. In Fig. 5 the results for the TT angular power spectra are illustrated. In both plots the full lines denote the analytical estimate while the dashed lines represent the numerical result. In Fig. 5, from left to right, the magnetic field intensity and the spectra index increase. In both plots of Fig. 5 the dot-dashed lines denote the WMAP 5yr best fit. The results illustrated in Fig. 5 are representative of a general trend which has been observed also in other cases and can be summarized as follows:

- the analytic result for the TT correlations stemming from the basic integrals studied in this paper always underestimates the numerical result;
- the analytic result becomes progressively inaccurate as the field strength increases above 10 nG.

Various other examples show that the polarization autocorrelations (i.e. the EE angular power spectra) are better captured by the analytical results, as already shown in Figs. 3 and 4. The temperature-polarization cross-correlations (i.e. the TE angular power spectra) share the same levels of accuracy of the TT correlations and they are illustrated in Fig. 6. As in Fig. 5 the dot-dashed lines denote the best fit to the WMAP 5yr data alone. For $B_L \leq 10$ n G the analytic results are rather accurate for the TT, TE and EE angular power spectra. In the case $B_L > 10$ nG the results become progressively less accurate in the case of the TT and TE correlations but remain reasonable for the EE autocorrelations.

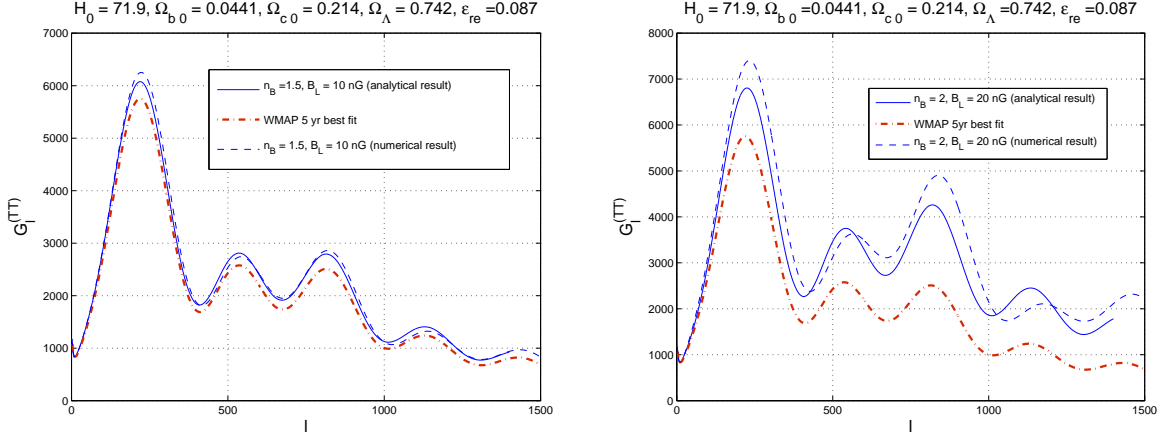


Figure 5: The semi-analytic results for the temperature autocorrelations are illustrated in the case $\beta = 0$.

5.3 Envelopes and wiggles

Having tested the accuracy of the analytical results, the handiness of the approach developed in the present investigation resides in the determination of the scaling properties of the various correlation functions. To proceed in this direction, the idea is to compute numerically

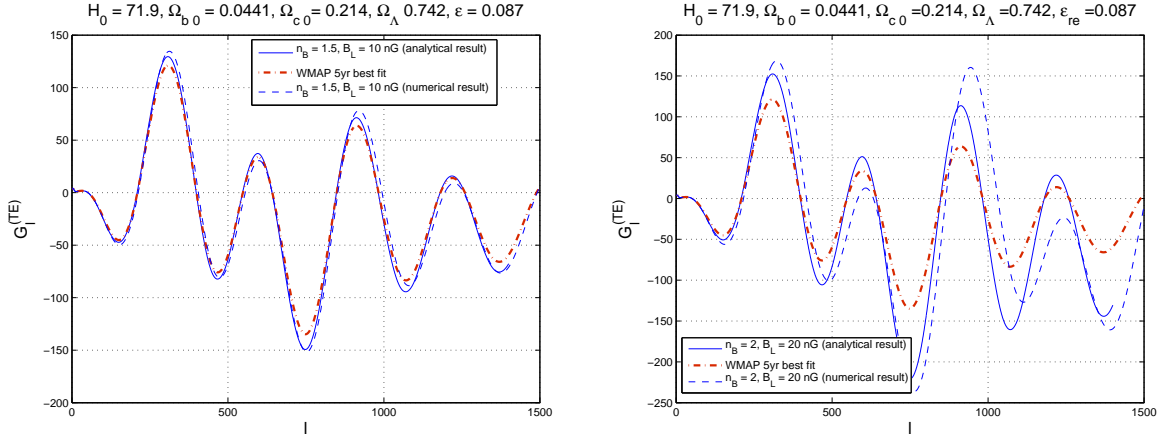


Figure 6: The semi-analytic results for the temperature-polarization cross-correlations are illustrated always in the case $\beta = 0$.

the ratios

$$R_\ell^{(TT)} = \frac{G_\ell^{(TT)}(n_B, B_L)}{G_\ell^{(TT)}}, \quad R_\ell^{(EE)} = \frac{G_\ell^{(EE)}(n_B, B_L)}{G_\ell^{(EE)}}, \quad (5.11)$$

where, by definition, $G_\ell^{(TT)}$ and $G_\ell^{(EE)}$ denote the angular power spectra in the absence of ambient magnetic field. The same procedure can be carried on also for the TE correlations.

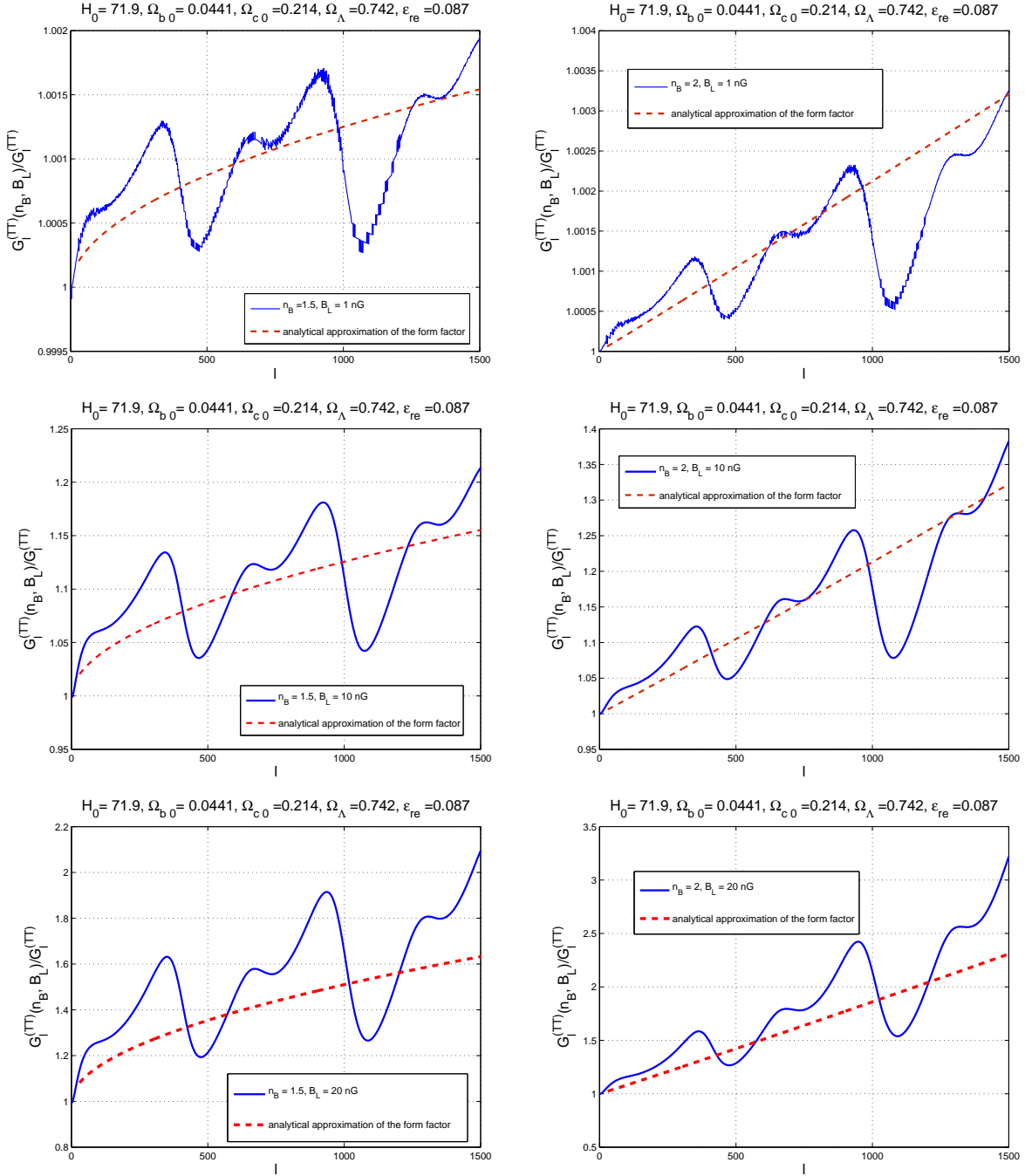


Figure 7: The magnetized form factor from the TT correlations for different values of the magnetic field background. The correlation angle is fixed to $\beta = 0$.

However, since the TE correlations are not positive definite and pass through zero, the resulting plots are not as revealing as the ones obtainable from the TT and EE angular power spectra. Figures 7 and 8 illustrate, respectively, $R_\ell^{(TT)}$ and $R_\ell^{(EE)}$ for different values of the magnetic field intensities and for different values of the spectral indices. The ratios

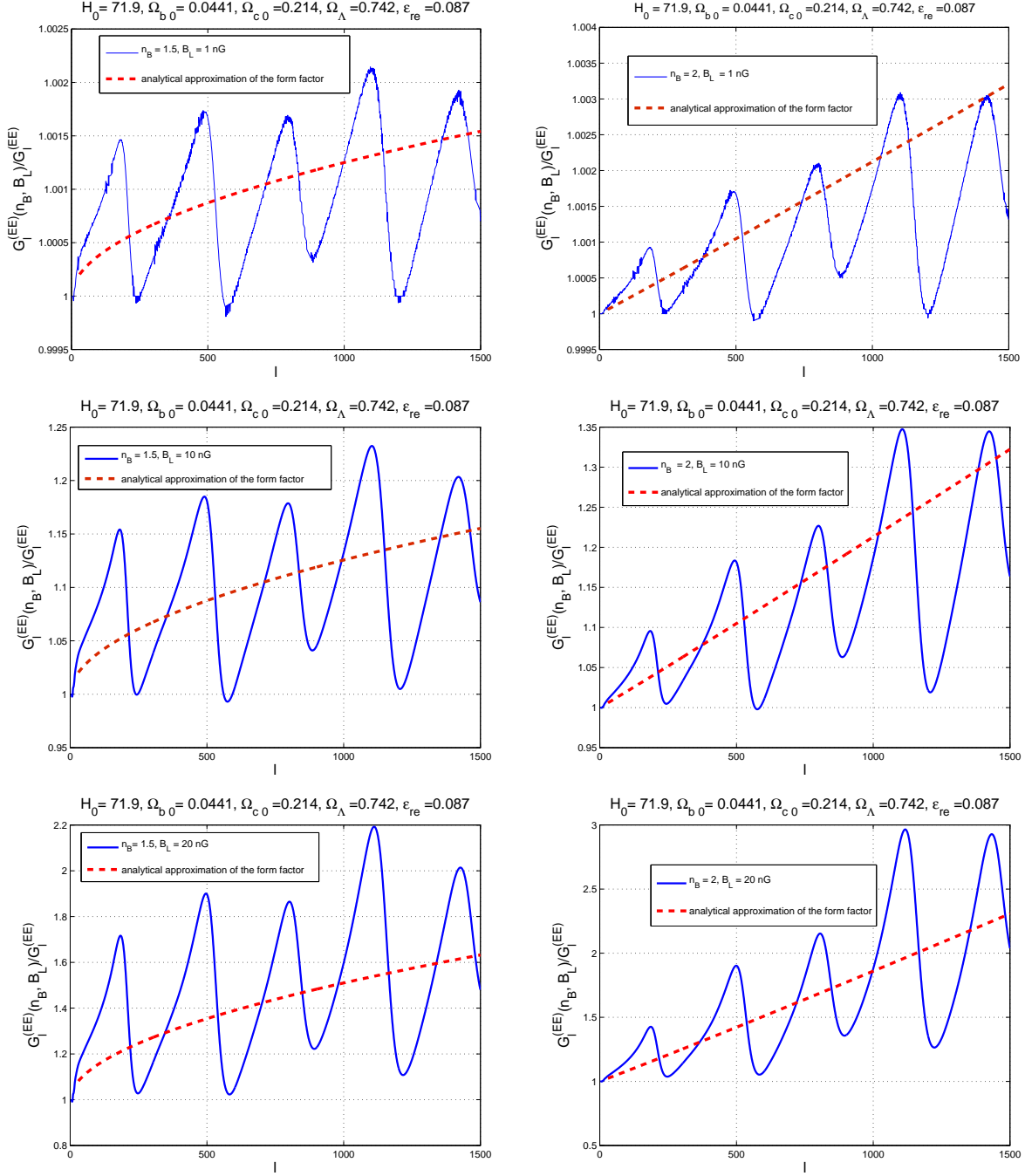


Figure 8: The magnetized form factor from the EE correlations for different values of the magnetic field background. The correlation angle is fixed to $\beta = 0$.

$R^{(TT)}$ and $R^{(EE)}$ represent an effective numerical diagnostic of the possible influence of a putative magnetic field. Indeed the diffusive scales, the thickness of the last scattering surface the optical depth at reionization are only mildly sensitive to the presence of an ambient magnetic field. The analytic structure of the angular power spectra computed in

section 4 suggests the possibility of factorizing the effects of a putative magnetic field into an appropriate form factor which is, incidentally, illustrated in Figs. 7 and 8 with a dashed line. On a qualitative ground the form factor represents, in some sense, the average of $R_\ell^{(XY)}$. On a more quantitative ground the results of section 4 suggest that $R_\ell^{(XY)}$ can be factorized into the product of a non-oscillating factor (i.e. $\overline{F}_\ell(n_B, B_L)$) and of an oscillating contribution (i.e. $\mathcal{O}_\ell^{(XY)}(n_s, n_B, \mathcal{A}_R, B_L)$). Therefore, within the notations followed in the present paper, we will have that $R_\ell^{(XY)}$ can be written as

$$R_\ell^{(XY)}(n_B, B_L, n_s, \mathcal{A}_R) = \overline{F}_\ell(n_B, B_L) \mathcal{O}_\ell^{(XY)}(n_s, n_B, \mathcal{A}_R, B_L). \quad (5.12)$$

where $X, Y = T, E$. The result for the magnetic form factor is

$$\overline{F}_\ell(n_B, B_L) = 1 + a_1 \left(\frac{B_L}{\text{nG}} \right)^4 \mathcal{J}_1(n_s, n_B, \ell) + a_2 \left(\frac{B_L}{\text{nG}} \right)^2 \mathcal{J}_2(n_s, n_B, \beta, \ell). \quad (5.13)$$

Within the set of parameters given by Eq. (5.9) the constants a_1 and a_2 are given by

$$a_1 = 1.393 \times 10^{-7}, \quad a_2 = 1.952 \times 10^{-3}, \quad (5.14)$$

while the functions $\mathcal{J}_1(n_s, n_B, \ell)$ and $\mathcal{J}_2(n_s, n_B, \beta, \ell)$ can be expressed as

$$\mathcal{J}_1(n_s, n_B, \ell) = \left(\frac{k_0}{k_L} \right)^{2(n_B-1)} \left(\frac{k_0}{k_p} \right)^{(1-n_s)} \left(\frac{2\ell}{\ell_B} \right)^{2n_B-n_s-1} \Sigma_1(n_s, n_B), \quad (5.15)$$

$$\mathcal{J}_2(n_s, n_B, \beta, \ell) = \cos \beta \left(\frac{k_0}{k_L} \right)^{(n_B-1)} \left(\frac{k_0}{k_p} \right)^{(1-n_s)/2} \left(\frac{2\ell}{\ell_B} \right)^{\frac{2n_B-n_s-1}{2}} \Sigma_2(n_s, n_B). \quad (5.16)$$

In Eqs. (5.15) and (5.16) the functions $\Sigma_1(n_s, n_B)$ and $\Sigma_2(n_s, n_B)$ encode a milder dependence upon the spectral indices and they can be determined by matching the Sachs-Wolfe expression (valid for $\ell < \ell_1$) with the results of the explicit numerical integration of the basic integrals (valid for $\ell > \ell_1$). The form of $\Sigma_1(n_s, n_B)$ and $\Sigma_2(n_s, n_B)$ also depend upon the regularization scheme of the magnetic energy density and here the explicit expressions will be given in the case of blue magnetic spectral indices:

$$\Sigma_1(n_s, n_B) = \frac{\Gamma^2(2 - n_s/2)}{\Gamma(3 - n_s)\Gamma^2(5/2 - n_B)} f(n_B - 1). \quad (5.17)$$

$$\Sigma_2(n_s, n_B) = \frac{\Gamma\left(\frac{7}{2} - \frac{n_s}{2} - n_B\right) \Gamma^2(2 - n_s/2)}{\Gamma^2\left(\frac{9}{4} - \frac{n_s}{4} - \frac{n_B}{2}\right) \Gamma(3 - n_s)} \sqrt{f(n_B - 1)}, \quad (5.18)$$

$$f(x) = \frac{4(6 - x)(2\pi)^{2x}}{3x(3 - 2x)\Gamma^2(x/2)}. \quad (5.19)$$

$$(5.20)$$

The functions appearing in Eqs. (5.17)–(5.18) can also be estimated (just in the limit of large ℓ) from the analytic expressions of the different integrals, as illustrated above in this

section. In the latter case the resulting expression will still have the correct scaling properties but the overall normalization will have to be adjusted. Conversely, the advantage of Eqs. (5.15)–(5.16) and (5.17)–(5.18) is that they are immediately comparable to the numerical calculation also for small ℓ . In Eqs. (5.15) and (5.16) we have that $\ell_B = 1$. If the integrals would just be estimated from their small-scale approximation the putative value of ℓ_B would be larger and will fix the limits of applicability of the formula.

As already mentioned, in Figs. 6 and 7 the dashed curves illustrate the magnetic form factor of Eq. (5.13) for the different values of the parameters appearing in each plot. The structure of Figs. 7 and 8 is as follows:

- in the three plots at the left the magnetic spectral index is fixed to $n_B = 1.5$ while in the three plots at the right the magnetic spectral index is fixed to $n_B = 2$;
- from top to bottom, as indicated in each plot, the values of the magnetic field intensity augments from 1 nG to 20 nG.

According to Figs. 7 and 8, the magnetic form factor of Eq. 5.13 reproduces quite faithfully the average of the numerical data and this is what scaling relations can provide, in this context. As explicitly shown by Figs. 7 and 8 the very same form factor works both for the TT and for the EE angular power spectra. The latter observation demonstrates that the factorization of Eq. (5.12) is not only analytically plausible but it is also numerically justified. The last observation brings up a further question: can we also understand semi-

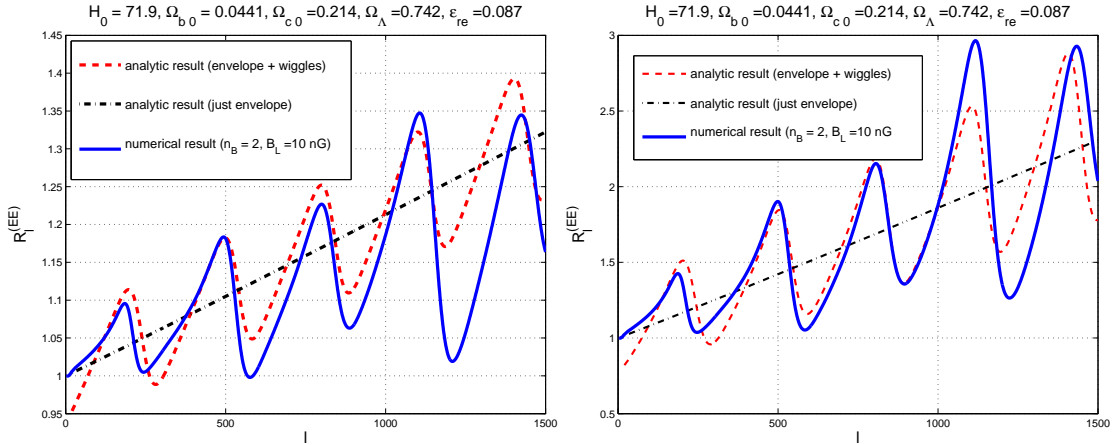


Figure 9: The analytic form of the wiggles is compared with the numerical results.

analytically the structure of the wiggles of Figs. 7 and 8? While in Fig. 9 the wiggles exhibit a double periodicity (i.e. a hump is followed by a peak), in Fig. 8 there is a single periodicity (i.e. a single peak is followed by a single peak). The difference in the two structure is understandable on the basis of the considerations of sections 3 and 4: while the TT correlations arise as the interference of the monopole and of the dipole ther EE

correlations mainly feel the dipole and are, therefore, a cleaner probe where the analytic considerations can be more easily confronted with the numeric results. Going back to the parametrization of Eq. (5.12) the analytic structure of the wiggles can be written as

$$O^{(EE)}(n_B, B_L) = \frac{a_E - b_E \cos [2\gamma_A(\ell + \ell_1) - \delta_B]}{a_E - b_E \cos [2\gamma_A(\ell + \ell_1)]}. \quad (5.21)$$

$$\delta_B \equiv \delta(n_B, B_L) = 9.2 \times 10^{-3} \left[\left(\frac{B_L}{\text{nG}} \right)^2 + \frac{2n_B - n_s - 1}{2} \left(\frac{B_L}{\text{nG}} \right) \right], \quad (5.22)$$

where ℓ_1 , a_E and b_E have been already introduced in Eqs. (5.6)–(5.7). The rationale behind Eqs. (5.21)–(5.22) is rather simple. In the denominator of Eq. (5.21) there is the analytic form of the best fit, while in the numerator the ambient magnetic field introduces a phase difference. In Fig. 9 the analytic expressions for the wiggles are compared with the numerical results. The remaining offsets are within the accuracy of the analytic approach and improve on the pure scaling estimate which lead to the derivation of the envelope. The results derived here are relevant for the dedicated strategies of parameter extraction which have been suggested in [62].

6 Parameter space of magnetized CMB observables

In the present study the values of the magnetic field intensities and of the corresponding spectral indices have been taken to be, in some cases, rather large in the sense that the selected values lead to CMB observables which are incompatible with the observed ones. As already mentioned the largeness of some of the selected values is evident from the comparison of the computed CMB observables with the best fit to the WMAP 5yr data alone (see, e.g. Fig. 2)

The choice of dealing with some of these extreme values is, in some sense, dictated by the logic followed in the present study: for large values of the magnetic fields, the scaling properties of the angular power spectra are more transparent and the distortions enhanced. We hope it is clear, from the results of the previous section, that indeed, the distortion patterns scale with the amplitude but their morphology remains unchanged. This is, after all, closely related to the intuitive notion of scaling (see, e.g. Figs. 7 and 8).

At the beginning of Section 2 it has been mentioned that, for instance, the values $(n_B, B_L) = (2, 10 \text{ nG})$ are excluded, in a frequentist perspective, to 95 % confidence level. In what follows the latter statement will be made more quantitative by deriving and by discussing the relevant exclusion plots in terms of the spectral index n_B and of the magnetic field intensity B_L . Let us, first of all, convince ourselves that, indeed, the model $(n_B, B_L) = (2, 10 \text{ nG})$ does not correctly reproduce the data. In Fig. 10 the full line illustrates the best fit to the WMAP 5yr data alone while the dashed line is the numerical result for the case $(n_B, B_L) = (2, 10 \text{ nG})$, when all the other parameters are fixed as in Eq. (5.9). If Fig. 10 the data points (with the corresponding error bars) refer to the binned data both

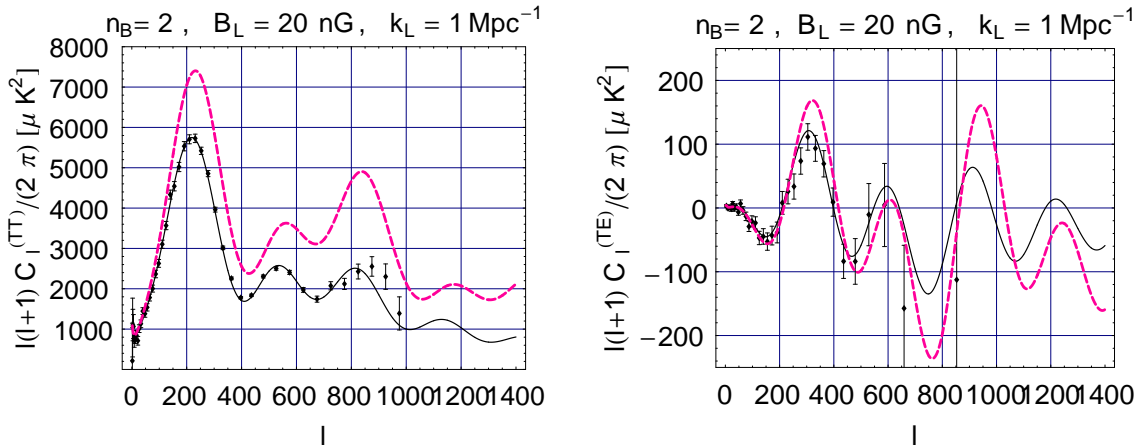


Figure 10: The TT and TE angular power spectra are illustrated in the case $(n_B, B_L) = (2, 10 \text{ nG})$ (dashed lines) and for the best fit to the WMAP 5yr data alone (full line). In both cases $\beta = 0$ for consistency with the analysis of the previous sections.

for the TT and TE angular power spectra. The binned data contain 34 (effective) multipoles in the TE correlation and 43 (effective) multipoles in the TT spectrum. Following the usual habit, to make the plots more readable, the binned data points have been included. Conversely, the unbinned data (which are the ones used in the following analyses) contemplate all the multipoles from $\ell = 2$ to $\ell = 1000$ both for the TT and for the TE (observed) power spectra. Finally, we included the TT and the TE angular power spectra since they are the best measured spectra in the context of the WMAP 5yr data.

Having established that the parameters $(n_B, B_L) = (2, 10 \text{ nG})$ are excluded let us now try to understand to what confidence level they can be excluded. The simplest way of exploring the parameter space of the magnetized models goes, in short, as follows:

- the joined two-dimensional marginalized contours for the various cosmological parameters identified already by the analyses of the WMAP 3yr data are ellipses with an approximate Gaussian dependence on the confidence level;
- the confidence intervals for the 2 supplementary parameters of the model (i.e. n_B, B_L) can then be determined by using an appropriate gridding approach;
- the remaining parameters of Eq. (5.9) are assumed to be known and follow a Gaussian probability densityfunction.

This approach is rather standard when exploring the impact of new scenarios on the CMB observables (see, e.g., [50, 51, 54] for the case of non-adiabatic modes supplementing the standard Λ CDM scenario). In the approach we just described, the shape of the likelihood

function can be determined by evaluating the least square estimator

$$\chi^2(n_B, B_L) = \sum_{\ell} \left[\frac{C_{\ell}^{(\text{obs})} - C_{\ell}(n_B, B_L)}{\sigma_{\ell}^{(\text{obs})}} \right]^2, \quad (6.1)$$

where $\sigma_{\ell}^{\text{obs}}$ are the estimated errors from the observations for each multipole and where the functional dependence of $C_{\ell}(n_B, B_L)$ is given by the underlying theory (i.e. the magnetized Λ CDM model) which we try to falsify by comparing its predictions to the actual observations. The observed angular power spectra (i.e. C_{ℓ}^{obs}) are derived by using the (further) estimators $\hat{C}_{\ell}^{(\text{TT})}$ and $\hat{C}_{\ell}^{(\text{TE})}$, i.e.

$$\hat{C}_{\ell}^{(\text{TT})} = \frac{1}{2\ell + 1} \sum_{m=-\ell}^{\ell} |\hat{a}_{\ell m}^{(\text{T})}|^2, \quad \hat{C}_{\ell}^{(\text{TE})} = \frac{1}{2\ell + 1} \sum_{m=-\ell}^{\ell} |\hat{a}_{\ell m}^{(\text{T})} \hat{a}_{\ell m}^{(\text{E})*}|, \quad (6.2)$$

whose distribution becomes Gaussian, according to the central limit theorem, when $\ell \rightarrow \infty$. The minimization of Eq. (6.1) is equivalent to the minimization of the lognormal likelihood function $\mathcal{L} = -2 \ln L$ where L is given by

$$L(\text{data} | n_B, B_L) = L_{\text{max}} e^{-\chi^2(n_B, B_L)/2}. \quad (6.3)$$

Thus, the minimization of Eq. (6.1) is equivalent to the maximization of the likelihood of Eq. (6.3). In Fig. 11 the parameter space of the model is illustrated, respectively, for

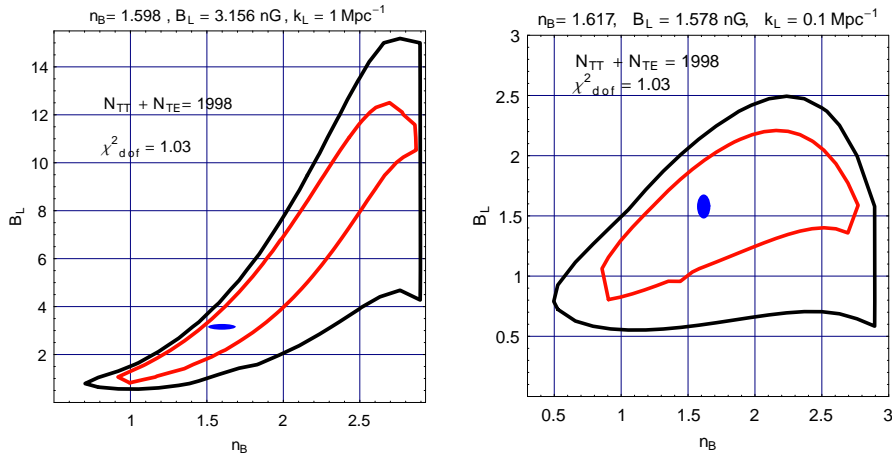


Figure 11: The parameter space of the magnetized CMB anisotropies for two illustrative choices of the magnetic pivot scale. In both plots $\beta = 0$.

two different choices of the magnetic pivot scale k_L , i.e. $k_L = \text{Mpc}^{-1}$ (plot at the left) and $k_L = 0.1 \text{ Mpc}^{-1}$ (plot at the right). The shaded spots, in both plots of Fig. 11, are meant to emphasize the value for which the estimator of Eq. (6.1) is minimized; note that $\chi^2_{\text{dof}} = \chi^2_{\text{min}}/N_{\text{dof}}$ is the value of the (reduced) χ^2 at the minimum (i.e. when $\chi^2 \equiv \chi^2_{\text{min}}$). In both plots the data points for the TE and TT angular power spectra have been used

in their unbinned form. Overall the total number of data points is $N_{\text{TT}} + N_{\text{TE}} = 1998$ since $N_{\text{TT}} = 999$ and $N_{\text{TE}} = 999$. In both plots of Fig. 11 the boundaries of the two regions contain 68.3% and 95.4% of likelihood as the values for which the χ^2 has increased, respectively, by an amount $\Delta\chi^2 = 2.3$ and $\Delta\chi^2 = 6.17$. The latter figures stem directly from the fact that we are dealing with a two-dimensional parameter space. Figure 11 offers a more quantitative interpretation of the plots reported in Fig. 10. In Fig. 10 the value of the magnetic pivot scale is $k_L = \text{Mpc}^{-1}$. Therefore the results of Fig. 11 do apply. In Fig. 11 the point $(n_B, B_L) = (2, 10 \text{ nG})$ is located very far from the outer contour. In a frequentist perspective, a model located beyond the outer contours of Figs. 11 is excluded, by the current WMAP data on the TT and TE correlations, to 95% confidence level.

The exclusion plots reported in Fig. 11 have been obtained by means of a grid approach and by using directly the numerical results. We can now ask ourselves the following question. What happens if we use the approximate form of the angular power spectra derived in the present paper and use, simultaneously, the same data but in their binned form? The results

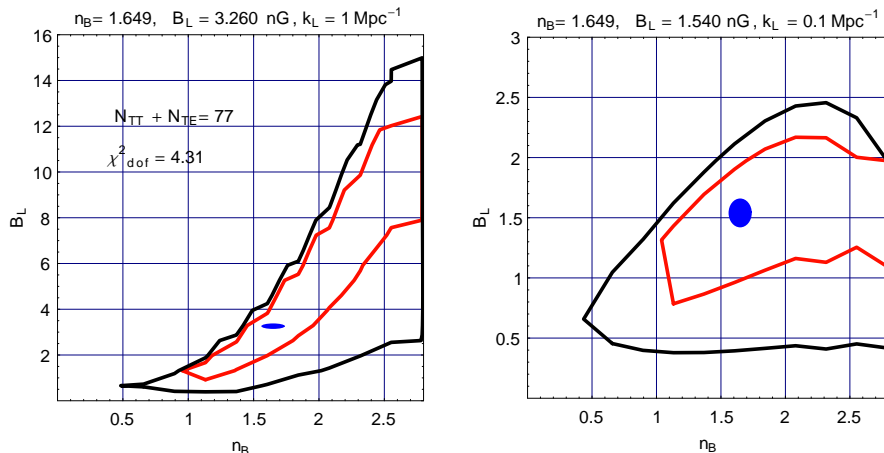


Figure 12: The parameter space of the magnetized CMB anisotropies as derived by using the semi-analytic expressions for the angular power spectra together with the data in their binned form. In both plots $\beta = 0$.

are illustrated in Fig. 12. It is amusing to notice that, in spite of numerical differences which are fully justified the shapes and the regions of the exclusion plots of Fig. 12 are consistent with the ones of Fig. 11. The results of Fig. 12 have been obtained by parametrizing the angular power spectra as in Section 5. Note, however, that in Section 5 we only reported explicit expressions in the case $n_B > 1$. To obtain the result of Fig. 12 we also need the analog formulas but in the case¹⁴ $n_B < 1$. The results of Fig. 12 show a fair consistency of our analytical approach. At the same time it is clear that the value of the reduced χ^2 is larger than in the case of Fig. 11: in Fig. 12, the data have been used in their binned

¹⁴Recall, as stressed in [60] (third paper in the reference), that the cases $n_B = 1$ and $n_B = 5/2$ should be separately regularized at the level of the magnetic energy density.

form. The largeness of the reduced χ^2 simply means, within the present approach, that the uncertainties entering Eq. (6.1) have been underestimated. With the last proviso, the results derived in this paper seem to allow for approximate evaluations of the parameter space of the magnetized CMB anisotropies which are compatible with the fully numerical results.

7 Concluding considerations

The (limited) question addressed in this paper is how the angular power spectra of the CMB anisotropies scale with the parameters of an ambient magnetic field when the remaining parameters are close to the ones of the standard Λ CDM scenario.

To get a definite answer, the calculation of the magnetized temperature and polarization anisotropies had to be reduced to the evaluation of a set of basic integrals whose explicit form simplifies in the limit of sufficiently small angular scales, i.e. in the limit of sufficiently large multipoles. It has been shown that the temperature and polarization observables obtainable by semi-analytic means are sufficiently accurate to infer a set of scaling relations which can be used to determine the effect of large-scale magnetic fields on the TT, TE and EE angular power spectra. It has been also shown explicitly how the distortions patterns induced by large-scale magnetism can be deduced from generalized magnetic form factors accounting for the scaling properties of the CMB observables as a function of the parameters of the ambient magnetic field.

The cleanest probe of large-scale magnetism is represented by the polarization autocorrelations. Indeed the magnetized EE angular power spectra exhibit a single periodicity, a milder dependence upon the dissipative scale and a rather clear shift of the peaks for intermediate and large multipoles. The obtained results have been confronted with the numerical calculation. The same evolution equations studied analytically have been integrated numerically. The analytical derivations are corroborated by the numerical results which are based on the same physical description. The obtained results are relevant for dedicated strategies of parameter extraction such as the ones mentioned at the end of the previous section.

Large-scale magnetism is a complicated phenomenon which we choose to scrutinize in its infancy, i.e. around the time of photon decoupling. This analysis must necessarily be cautious and modest. The rationale for such a caveat does not reside in a particular ethical conviction but in the nature of the problem: while in the laboratory we completely dominate the initial conditions of our experiments in astrophysics and cosmology this is not the case. So, unless we are vigilant it is well possible to mistake an effect due to the peculiar nature of initial conditions with a missing piece of dynamics which should have been included in a particular regime¹⁵. In this respect it is important to understand in detail all the potentially

¹⁵By this statement I mean that it is important to scrutinize systematically all the relevant plasma effects which are applicable in the pre-decoupling regimes. This has been partially done in the present paper as well as the original studies of Refs. [44, 45, 46, 49]. Even if the present estimates suggest that other (potentially relevant) plasma effects do not play a crucial numerical role, care must be taken in sharpening these estimates.

interesting physical effects which could modify the CMB observables. This study is time-consuming both at a numerical and at the analytic level. It could even be said, by some, that such an approach is slow and pedantic. While we are ready to take this risk, it is rewarding that, at the moment, the estimates of the effects of large-scale magnetism on the scalar modes of the CMB anisotropies seem to reach (slowly) the same standards employed in the absence of ambient magnetic fields. More theoretical effort, in this direction, is certainly needed.

Indeed, a missing piece of the dynamics could be mistaken as a peculiar feature stemming from the initial conditions.

References

- [1] G. Hinshaw *et al.* [WMAP Collaboration], arXiv:0803.0732 [astro-ph].
- [2] J. Dunkley *et al.* [WMAP Collaboration], arXiv:0803.0586 [astro-ph].
- [3] E. Komatsu *et al.* [WMAP Collaboration], arXiv:0803.0547 [astro-ph].
- [4] D. N. Spergel *et al.* [WMAP Collaboration], *Astrophys. J. Suppl.* **170**, 377 (2007).
- [5] L. Page *et al.* [WMAP Collaboration], *Astrophys. J. Suppl.* **170**, 335 (2007).
- [6] C. I. Kuo *et al.* [ACBAR collaboration], *Astrophys. J.* **600**, 32 (2004).
- [7] C. L. Kuo *et al.*, *Astrophys. J.* **664**, 687 (2007); C. L. Reichardt *et al.*, arXiv:0801.1491 [astro-ph].
- [8] C. Pryke *et al.* [QUAD collaboration], arXiv:0805.1944 [astro-ph].
- [9] E. Y. Wu *et al.* [QUaD Collaboration], arXiv:0811.0618 [astro-ph].
- [10] P. G. Castro *et al.* [QUaD collaboration], arXiv:0901.0810 [astro-ph.CO].
- [11] R. B. Friedman *et al.* [QUaD collaboration], arXiv:0901.4334 [astro-ph.CO].
- [12] M. Chu and L. Knox, *Astrophys. J.* **620**, 1 (2005).
- [13] M. Chu, M. Kaplinghat and L. Knox, *Astrophys. J.* **596**, 725 (2003).
- [14] M. Kaplinghat, L. Knox and C. Skordis, *Astrophys. J.* **578**, 665 (2002)
- [15] W. Hu, M. Fukugita, M. Zaldarriaga and M. Tegmark, *Astrophys. J.* **549**, 669 (2001).
- [16] M. Giovannini, *Int. J. Mod. Phys. D* **13**, 391 (2004).
- [17] M. J. Rees, *Lect. Notes Phys.* **664**, 1 (2005).
- [18] H. Alfvén, *Arkiv. Mat. F. Astr., o. Fys.* **29 B**, 2 (1943).
- [19] E. Fermi, *Phys. Rev.* **75**, 1169 (1949).
- [20] E. Fermi, *Nuovo Cim. Suppl.* **6**, 318 (1949).
- [21] H. Alfvén, *Phys. Rev.* **75**, 1732 (1949).
- [22] R. D. Richtmyer and E. Teller, *Phys. Rev.* **75**, 1729 (1949).
- [23] M. Giovannini, *Phys. Lett. B* **659**, 661 (2008).

- [24] K. Bamba, Phys. Rev. D **74**, 123504 (2006).
- [25] K. Bamba, C. Q. Geng and S. H. Ho, JCAP **0811**, 013 (2008).
- [26] L. Campanelli, arXiv:0805.0575 [astro-ph].
- [27] L. Campanelli, P. Cea, G. L. Fogli and L. Tedesco, Phys. Rev. D **77**, 123002 (2008).
- [28] Ya. Zeldovich, Sov. Phys. JETP **21**, 656 (1965).
- [29] E. Harrison, Phys. Rev. Lett. **18**, 1011 (1967).
- [30] E. Harrison, Mon. Not. R. Astr. Soc. **147**, 279 (1970).
- [31] M. Giovannini, Phys. Rev. D **62**, 123505 (2000).
- [32] W. A. Hiltner, Science **109**, 165 (1949); J. S. Hall, Science **109**, 166 (1949); L. J. Davis and J. L. Greenstein, Astrophys. J. **114**, 206 (1951).
- [33] A. A. Ruzmaikin, A. M. Shukurov, D. D. Sokoloff *Magnetic Fields of Galaxies*, (Kluwer Academic Publisher, Dordrecht, 1988).
- [34] R. Beck, Astron.Nachr. **327**, 512 (2006); R. Beck, A. Brandenburg, D. Moss, A. Skhurov, D. Sokoloff, Annu. Rev. Astron. Astrophys. **34**, 155 (1996).
- [35] C. L. Carilli and G. B. Taylor, Ann. Rev. Astron. Astrophys. **40**, 319 (2002).
- [36] K. T. Kim, P. C. Tribble and P. P. Kronberg, Astrophys. J. **379**, 80 (1991); T.E. Clarke, P.P. Kronberg and H. Böhringer, *Astrophys. J.* **547**, L111 (2001).
- [37] A. Loeb, JCAP **0703**, 001 (2007).
- [38] P. P. Kronberg, R. Kothes, C. J. Salter and P. Perillat, Astrophys. J. **659**, 267 (2007).
- [39] M. L. Bernet, F. Miniati, S. J. Lilly, P. P. Kronberg and M. Dessauges-Zavadsky, arXiv:0807.3347 [astro-ph].
- [40] L. Spitzer, *Physics of Fully ionized plasmas* (J. Wiley and Sons, New York, 1962).
- [41] N. A. Krall, A. W. Trivelpiece: *Principles of Plasma Physics*, (San Francisco Press, San Francisco 1986).
- [42] D. Biskamp, *Non-linear Magnetohydrodynamics* (Cambridge University Press, Cambridge, 1994).
- [43] T. J. M Boyd, J. J. Serson: *The physics of plasmas*, (Cambridge University Press, Cambridge, UK, 2003).

- [44] M. Giovannini, Phys. Rev. D **73**, 101302 (2006).
- [45] M. Giovannini, Phys. Rev. D **70**, 123507 (2004).
- [46] M. Giovannini, Phys. Rev. D **74**, 063002 (2006).
- [47] M. Giovannini, Class. Quant. Grav. **23**, R1 (2006).
- [48] M. Giovannini, PMC Phys. A **1**, 5 (2007); M. Giovannini and K. Kunze, Phys. Rev. D **77**, 061301 (2008); Phys. Rev. D **77**, 063003 (2008).
- [49] M. Giovannini, Class. Quant. Grav. **23**, 4991 (2006); M. Giovannini and K. Kunze, Phys. Rev. D **77**, 123001 (2008).
- [50] K. Enqvist and H. Kurki-Suonio, Phys. Rev. D **61**, 043002 (2000).
- [51] K. Enqvist, H. Kurki-Suonio and J. Valiviita, Phys. Rev. D **62**, 103003 (2000).
- [52] H. Kurki-Suonio, V. Muhonen and J. Valiviita, Phys. Rev. D **71**, 063005 (2005).
- [53] J. Valiviita and V. Muhonen, Phys. Rev. Lett. **91**, 131302 (2003).
- [54] R. Keskitalo, H. Kurki-Suonio, V. Muhonen and J. Valiviita, JCAP **0709**, 008 (2007).
- [55] K. Subramanian and J. D. Barrow, Phys. Rev. Lett. **81**, 3575 (1998).
- [56] K. Subramanian and J. D. Barrow, Phys. Rev. D **58**, 083502 (1998).
- [57] K. Subramanian and J. D. Barrow, Mon. Not. Roy. Astron. Soc. **335**, L57 (2002).
- [58] C. Tsagas and R. Maartens, Phys. Rev. D **61**, 083519 (2000).
- [59] J. D. Barrow and C. G. Tsagas, arXiv:0803.0660 [astro-ph].
- [60] M. Giovannini, Phys. Rev. D **56**, 3198 (1997); M. Giovannini and K. Kunze, Phys. Rev. D **78**, 023010 (2008); CERN-PH-TH-2008-232, arXiv:0812.2207 [astro-ph].
- [61] M. Giovannini, Phys. Rev. D **71**, 021301 (2005); M. Giovannini and K. E. Kunze, CERN-PH-TH-2008-233, arXiv:0812.2804 [astro-ph].
- [62] M. Giovannini, CERN-TH-PH/2009-028, arXiv:0902.4353 [astro-ph.CO].
- [63] J. M. Bardeen, Phys. Rev. D **22**, 1882 (1980).
- [64] R. A. Sunyaev and Y. B. Zeldovich, Astrophys. Space Sci. **7**, 3 (1970).
- [65] P. Naselsky and I. Novikov, Astrophys. J. **413**, 14 (1993); H. Jorgensen, E. Kotok, P. Naselsky, and I. Novikov, Astron. Astrophys. **294**, 639 (1995).

- [66] B. Jones and R. Wyse, *Astron. Astrophys.* **149**, 144 (1985).
- [67] M. Zaldarriaga, *Phys. Rev. D* **55**, 1822 (1997).
- [68] M. Abramowitz and I. A. Stegun, *Handbook of Mathematical Functions* (Dover, New York, 1972).
- [69] A. Erdelyi, W. Magnus, F. Obhehttinger, and F. Tricomi, *Higher Transcendental Functions* (Mc Graw-Hill, New York, 1953).
- [70] M. Zaldarriaga and U. Seljak, *Phys. Rev. D* **55**, 1830 (1997).
- [71] J. N. Goldberg *et al.*, *J. Math. Phys.* **8**, 2155 (1967).
- [72] M. Kamionkowski, A. Kosowsky and A. Stebbins, *Phys. Rev. D* **55**, 7368 (1997).
- [73] M. Zaldarriaga and D. D. Harari, *Phys. Rev. D* **52**, 3276 (1995)
- [74] U. Seljak and M. Zaldarriaga, *Astrophys. J.* **469**, 437 (1996).
- [75] U. Seljak, *Astrophys. J.* **435**, L87 (1994)
- [76] W. Hu and N. Sugiyama, *Astrophys. J.* **444**, 489 (1995);
- [77] W. Hu and N. Sugiyama, *Astrophys. J.* **471**, 542 (1996).
- [78] P. J. E. Peebles and J. T. Yu, *Astrophys. J.* **162** 815 (1970).
- [79] P. Astier *et al.* [The SNLS Collaboration], *Astron. Astrophys.* **447**, 31 (2006);
A. G. Riess *et al.* [Supernova Search Team Collaboration], *Astrophys. J.* **607**, 665 (2004).
- [80] D. J. Eisenstein *et al.* [SDSS Collaboration], *Astrophys. J.* **633**, 560 (2005).
- [81] U. Seljak and M. Zaldarriaga, *Astrophys. J.* **469**, 437 (1996).
- [82] M. Zaldarriaga, D. N. Spergel and U. Seljak, *Astrophys. J.* **488**, 1 (1997).
- [83] E. Bertschinger, *COSMICS* arXiv:astro-ph/9506070.
- [84] C. P. Ma and E. Bertschinger, *Astrophys. J.* **455**, 7 (1995)